AD- 400 266

HE-150-204
TECHNICAL REPORT

UNIVERSITY OF CALIFORNIA
INSTITUTE OF ENGINEERING RESEARCH
BERKELEY, CALIFORNIA

OPTICAL STRAIN MEASUREMENTS IN STAINLESS STEEL AT TRANSIENT TEMPERATURES TO 2000° F

by

Claude L. Arne

FACULTY INVESTIGATORS:
W. H. GIEDT, Professor of Aeronautical Sciences
J. FRISCH, Associate Professor of Mechanical Engineering

UCRL Purchase Order 1248500, UCX-2285

SERIES NO. 128
ISSUE NO. 9
DATE DECEMBER 20, 1962

PURCHASE ORDER 1243500
UCX-2285
REPORT NO. HE-150-204
SERIES NO. 128-9
DECEMBER 20, 1962

SPONSORED BY THE
LAWRENCE RADIATION LABORATORY
UNIVERSITY OF CALIFORNIA
LIVERMORE, CALIFORNIA

OPTICAL STRAIN MEASUREMENTS IN STAINLESS STEEL AT TRANSIENT TEMPERATURES TO 2000° F

by

Claude Lawrence Arne

A portion of a Master of Science Thesis
in Mechanical Engineering

FACULTY INVESTIGATOR:

W. H. GIEDT, Professor of Aeronautical Sciences
J. FRISCH, Associate Professor of Mechanical Engineering

APPROVED J. Frisch

ABSTRACT

Type 304 stainless steel plate specimens 0.24 x 2-1/4 x 4 inches in size were subjected to stagnation heating in an oxyacetylene flame apparatus. Transient thermal strains at temperatures up to 2000° F were measured with a modified Tuckerman optical strain gage shielded from heat transfer by a water cooled radiant heat shield. The general equations of thermoelasticity are developed for a flat homogeneous plate subjected to a particular transient three-dimensional temperature distribution. The experimentally determined temperatures in the specimens were used in the analytic solution for thermal strains which were found to agree very well with the optically measured strains on the unheated specimen surface.

TABLE OF CONTENTS

NOMENCLATURE

a,b,c,d,e f,g,h & i	temperature distribution constants
j	half length of specimen - 2.0 inches
k	half width of specimen - 1.125 inches
l,m,n	direction cosines
p	half thickness of specimen - 0.120 inches
q	space coordinate parallel to z-axis
r	space coordinate parallel to y-axis
s	space coordinate parallel to x-axis
t	time, seconds
u	arbitrary length parallel to x-axis
v	arbitrary length parallel to y-axis
x,y,z	cartesian space coordinates
E	Modulus of Elasticity, psi
G	Shear Modulus, psi
I	Moment of Inertia, inches^4
M	Moment, in.-lb.
T	Temperature, °F
X,Y,Z	Directions corresponding to x,y,z-axes

Greek Letters

α	coefficient of thermal expansion, in/in - °F
β	element axis (Fig. 6)
γ	shear strain component, in/in
ϵ	normal strain component, in/in
ζ	element axis (Fig. 6)

ν	Poisson's Ratio
σ	normal stress component, psi
τ	shear stress component, psi

Subscripts

x,y,z	directions parallel to cartesian space coordinates

LIST OF FIGURES

I. INTRODUCTION

Many technological advances have been made in recent years in the development of instrumentation for the measurement of temperature dependent physical properties. With the advances in nuclear and space technology there has been placed an ever increasing importance on those materials that can withstand extremely high temperatures. Before these sometimes new and exotic materials can be used there must be a thorough understanding of their physical properties when subjected to high temperatures.

There are many materials that can withstand high temperatures, but only a few are suitable as either nuclear or space system components. One reason for this is the high temperatures encountered during transient heating conditions, where the heating rates sometimes reach as high as 2,00 Btu/sec/ft^2. These heat fluxes produce large temperature gradients which cause failure if the temperature induced stress in the material exceeds a given failure criterion. The stress in a component part is directly related to the strain, and can be determined from strain measurements.

Generally when the temperature of a material will experience an expansion which is associated with the coefficient of thermal expansion for that particular material. When the temperature is raised under transient heating conditions there is generally a non-uniform and non-linear temperature distribution which results in a certain stress-strain distribution within the component part. With the material properties and the temperature distribution known, it is sometimes possible to determine the stress-strain distribution analytically. In many cases, however, where transient external loadings are applied or the geometrical

shape limits an analytical analysis, the strain at a particular location must be measured.

Although various techniques of strain measurement are widely used, methods for measuring strain when temperatures are above 1500° F are practically nonexistent. The most widely used method of measuring strain is the electrical strain gage, which is reliable up to 1500° F. Another method for obtaining strain measurements is the use of a Tuckerman optical strain gage.[15*] However, this strain gage is limited to a maximum temperature of 500° F, and under transient temperature rise the specimen surface is limited to about 1500° F (the extensometer having a much lower temperature, i.e., below 500° F).[2]

The objective of this project has been to develop a method whereby transient strain measurements with acceptable reliability for a specimen having a surface temperature up to 2000° F. After considering several ideas, it was decided that a procedure using existing equipment with certain modifications would give the desired results. The procedure adopted used the basic Tuckerman optical strain gage with a modification and a heat shield to prevent the extensometer from being heated above 500° F.

The oxyacetylene flame apparatus developed and used previously remained the same except that the hot gases were directed to give stagnation heating.[1,2,12,13,14] The important modification to the equipment was in the Tuckerman optical strain gage. This modification consisted of the attachment of copper tubing to the knife edge and lozenge of the extensometer. Water flowed through this copper tubing, preventing conduction of heat into the extensometer body. To prevent radiation heat

*NOTE: Numbers in superscript denote references listed in Bibliography.

transfer from the specimen surface to the extensometer body a water cooled heat shield was designed and built and placed between the extensometer and the specimen.

A specimen holding device was built to support the specimen free from external forces and to prevent vibration. A permanent record of the strain readings was obtained with a 16 mm movie camera.

The material used for the specimen plates was Type 304 stainless steel. This choice was made because of low thermal conductivity which gave larger temperature gradients than most metals, and because the properties were available in several references.

Since it would be necessary to support the experimental strain measurements with an analytical solution to show that large systematic errors were not present, a semi-analytical solution was developed from basic thermoelasticity and elasticity relationships. To develop this situation it was necessary to first determine the temperature distribution within the plate, using an existing technique.[1] With the three-dimensional transient temperature distribution known, the specimen was analyzed as a plane stress problem with elementary thermoelastic plate theory, elastic beam theory, and thermoelastic beam theory.

II. SEMI-ANALYTICAL DETERMINATION OF EXPANSION MEASURED BY EXTENSOMETER

The Type 304 stainless steel plate was subjected to nonuniform heating over its heated surface by an oxyacetylene flame. The resultant three-dimensional temperature distribution through the plate causes nonuniform expansion which can be analyzed by the general equations of thermoelasticity.

A. Basic Thermoelastic Equations

Solutions to three-dimensional problems of thermoelasticity must satisfy the familiar conditions of compatibility and the equations of equilibrium as well as the boundary conditions at the surfaces of the specimen. In terms of the cartesian coordinates x, y and z these equations with the body forces neglected are

Compatibility Conditions:

$$\frac{\partial^2 \epsilon_x}{\partial y^2} + \frac{\partial^2 \epsilon_y}{\partial x^2} = \frac{\partial^2 \gamma_{xy}}{\partial x\, \partial y}$$

$$\frac{\partial^2 \epsilon_y}{\partial z^2} + \frac{\partial^2 \epsilon_z}{\partial y^2} = \frac{\partial^2 \gamma_{xy}}{\partial y\, \partial z}$$

$$\frac{\partial^2 \epsilon_z}{\partial x^2} + \frac{\partial^2 \epsilon_x}{\partial z^2} = \frac{\partial^2 \gamma_{xz}}{\partial x\, \partial z}$$

$$2\frac{\partial^2 \epsilon_x}{\partial y \partial z} = \frac{\partial}{\partial x}\left[-\frac{\partial \gamma_{yz}}{\partial x} + \frac{\partial \gamma_{xz}}{\partial y} + \frac{\partial \gamma_{xy}}{\partial z}\right]$$

$$2\frac{\partial^2 \epsilon_y}{\partial x \partial z} = \frac{\partial}{\partial y}\left[\frac{\partial \gamma_{yz}}{\partial x} - \frac{\partial \gamma_{xz}}{\partial y} + \frac{\partial \gamma_{xy}}{\partial z}\right]$$

$$2\frac{\partial^2 \epsilon_z}{\partial x \partial y} = \frac{\partial}{\partial z}\left[\frac{\partial \gamma_{yz}}{\partial x} + \frac{\partial \gamma_{xz}}{\partial y} - \frac{\partial \gamma_{xy}}{\partial z}\right] \qquad (1)$$

Equilibrium Equations:

$$\frac{\partial \sigma_x}{\partial x} + \frac{\partial \tau_{xy}}{\partial y} + \frac{\partial \tau_{xz}}{\partial z} - \frac{\alpha E}{1-2\nu} \frac{\partial T}{\partial x} = 0$$

$$\frac{\partial \sigma_y}{\partial y} + \frac{\partial \tau_{xy}}{\partial x} + \frac{\partial \tau_{yz}}{\partial z} - \frac{\alpha E}{1-2\nu} \frac{\partial T}{\partial y} = 0 \qquad (2)$$

$$\frac{\partial \sigma_z}{\partial z} + \frac{\partial \tau_{xz}}{\partial x} + \frac{\partial \tau_{yz}}{\partial y} - \frac{\alpha E}{1-2\nu} \frac{\partial T}{\partial z} = 0$$

Boundary Conditions:

$$\sigma_x \ell + \tau_{xy} m + \tau_{xz} n = \frac{\alpha E T}{1-2\nu} \ell$$

$$\sigma_y m + \tau_{yz} n + \tau_{xy} \ell = \frac{\alpha E T}{1-2\nu} m \qquad (3)$$

$$\sigma_z n + \tau_{xz} \ell + \tau_{yz} m = \frac{\alpha E T}{1-2\nu} n$$

The foregoing equations are the basic relationships for elastic solids. Attainment of a solution that satisfies these conditions and equations would be exact and unique.[7]

Generally, the solution would be found in terms of stresses in the body, and Hooke's law is used to relate stresses to strains. For an isotropic elastic body the stress-strain equations for three-dimensional problems are[7]

$$\epsilon_x - \alpha T = \frac{1}{E} [\sigma_x - \nu (\sigma_y + \sigma_z)]$$

$$\epsilon_y - \alpha T = \frac{1}{E} [\sigma_y - \nu (\sigma_x + \sigma_z)] \qquad (4)$$

$$\epsilon_z - \alpha T = \frac{1}{E} [\sigma_z - \nu (\sigma_x + \sigma_y)]$$

$$\gamma_{xy} = \frac{\tau_{xy}}{G} \qquad \gamma_{yz} = \frac{\tau_{yz}}{G} \qquad \gamma_{xz} = \frac{\tau_{xz}}{G}$$

Using Equations (4) the six conditions of compatibility could be expressed in terms of the stresses. Since they are readily available[6] they are not repeated here.

B. Limited Application of Theoretical Equations of Thermoelasticity to Experimental Specimens

The specimen geometry is shown in Fig. 1. The axes are located to obtain symmetry about the point of intersection of the x, y, z axis in the midplane of the plate. This choice of location is based on the experimentally determined temperature distribution in the specimen interior. The large temperature gradients in the x-y plane, as shown in Figs. 15, 16 and 17, limit the usefulness of the basic equations of thermoelasticity whose linearity[2] nevertheless permits addition of the z-axis temperature distribution to the one in the x-y plane.

The large range in temperature (70° F to 2000° F) over which strains are measured means that the variation in mechanical properties such as the modulus of elasticity, coefficient of thermal expansion, and tensile yield strength, must be taken into account. These properties for Type 304 stainless steel are shown in Figs. 20, 22 and 23.

The limitation on the use of the thermoelasticity equations is due to the temperature gradients in the specimen causing the yield strength to be exceeded. This was confirmed by attempts to fit boundary conditions in the solution, as presented in the following sections. Depending upon the properties of the specimen, the method used in heating and the resulting temperature distribution, the thermoelastic equations can be used to obtain exact solutions, a number of which can be found in the literature.[2,3,4,5,6,7,17]

C. The Three-Dimensional Temperature Distribution

The results of the experimentally determined temperature distribution in Type 304 stainless steel specimens are shown in Figs. 15, 16 and 17, where the analytical results are shown by solid lines. A three-dimensional mathematical relationship describing the temperature distributions is used for substitution into the thermoelastic equations.

The temperature distribution is expressed by

$$T(x,y,z) = \frac{T_z}{a}(T_x - a) + \frac{T_z}{a}(T_y - a) + \frac{T_x T_y}{a^2}(T_z - a) + a \qquad (5)$$

where

$$T_x = a + bx^2 + cx^4 \qquad (6)$$

$$T_y = d + e \cos \frac{\pi y}{1.3} \qquad (7)$$

$$T_z = f + g(z+p) + h(z+p)^2 + i(z+p)^3 \qquad (8)$$

with the constants a through i generally having different values for each value of time, t. T_x and T_y represent the temperature distributions on the back surface of the plate for the respective x- and y-axes. T_z represents the temperature distribution along the z-axis at the x- and y-axes intersection. To determine the slope g of the temperature curve T_z at z = -0.120 inches, the heat flux measurement at the x-y axes intersection, Fig. 21, as well as the thermal conductivity of Type 304 stainless steel were used.

D. Solution for the Three-Dimensional Temperature Distribution

The strain measured by the Tuckerman optical strain gage was for a small area in the center of the plate specimen, as shown in Fig. 1. The average expansion over this area was found from the approximation of

adding to the free thermal expansion of the back surface of the plate the strain found from the free beam and plate analyses equations. The plate being free of initial residual stresses and external loads is analyzed as a plane stress problem.

The analysis of the plate is separated into two sections. In the first the back surface stress resulting from the temperature distribution in the z-direction is determined. In the second the stress distribution on the back surface of the plate (the x-y plane with $z = 0.120$ inch) is determined. The two solutions are then added to obtain the stress distribution for the area of measurement which is permissible because of the linearity of the thermoelastic equations.[2]

E. Solution for z-Axis Temperature Distribution

The plate was subjected in its interior to a temperature distribution given by Eqn's (5), (6), (7) and (8). For the small area on the back surface of the plate over which the stresses are to be determined these equations are essentially independent of T_x and T_y. The temperature distribution through the thickness then becomes

$$T(z) = T_z = f + g(z+p) + h(z+p)^2 + i(z+p)^3 \qquad (9)$$

The solution for this temperature distribution is given by Timoshenko,[7] who arrived at the solution by physical arguments involving the application and removal of boundary forces. The same solution is derived by Boley and Weiner,[6] who used a more rigorous semi-inverse approach. The solution leads to the following expressions for the stresses in the plate:[6]

$$\sigma_x = \sigma_y = \frac{1}{1-\nu} \left(- \alpha E T_z + \frac{N_T}{2p} + \frac{12 M_T}{8\, p^3} z \right) \tag{10}$$

$$N_T = \int_{-p}^{p} \alpha E T_z \, dz \tag{11}$$

$$M_T = \int_{-p}^{p} \alpha E T_z \, z \, dz \tag{12}$$

This solution is not correct at the edges of the plate, since the stresses do not vanish there. However, by St. Venant's principle, and since the area of interest is at the center of the plate, the stresses calculated will be correct.

Note that the above relationships take into account the variation of the properties with temperature as shown in Figs. 20 and 22. A comparison of the two figures shows that the product of the coefficient of expansion and the modulus of elasticity remains nearly constant over the range of temperature for each value of time, and that the variation is less than 2 per cent from the average. For this reason the product αE is set constant and removed to the outside of Eq. (10). For each specific value of time the average of αE is used in the calculations.

F. Stress Resulting from the Temperature Distribution in the x-y Plane

The subsequent analysis in this section is for the temperature distribution on the back surface of the plate ($z = t$). From Eq.(5) the expression describing this distribution is

$$T(x,y,p) = T_x + T_y - a \tag{13}$$

where $T_x = a + bx^2 + cx^4$ (6)

$$T_y = d + e \cos \frac{\pi y}{1.3} \tag{7}$$

The temperature distributions $T(x,o,p)$ are shown in Fig. 16, and the temperature distributions $T(y,o,p)$ are shown in Fig. 17. The symmetry of these temperature distributions is easily recognizable and the solution can therefore be reduced to the determination of the stresses for one quadrant of the plate.

The analyzed plate quadrant is bounded by the coordinate values $x = 0, j$ and $y = 0, k$. The boundary conditions on this quadrant are: 1) the x-axis remains fixed and undistorted; 2) the y-axis remains fixed and undistorted; 3) the x-axis and y-axis remain perpendicular; 4) the shear forces at $x = 0, j$ and $y = 0, k$ remain equal to zero; 5) the edges at $x = + j$ and $y = k$ are free to expand and have zero stress perpendicular to their edges; and 6) the moment forces at $x = + j$ and $y = k$ remain equal to zero. In addition, the warpage of the x-y plane is assumed negligible.

The first step in the analysis is the plotting of the temperature distributions for the quadrant of the plate. These plots for $x = 0$, 1.0", 1.5", and 2", and $y = 0$, 0.4", 0.8", and 1.125" for various times were made and a representative graph is shown in Fig. 18. Considering the trend of these temperature distributions, an element of the plate quadrant is shown in Fig. 7 with its displacements after heating has taken place. The displacements $\delta u_{\alpha T}$ and $\delta v_{\alpha T}$ represent the thermal expansion of the plate. the displacements δu_{σ} and δv_{σ} represent the strains due to the stress distribution in the plate. The thermal expansion of the back surface is determined from the temperature distribution.

To analyze the plate quadrant it has been duplicated by two fixed end beams. One beam is described by: a) the x-y axis intersect

being held fixed; b) free expansion being allowed parallel and along the x-axis; c) the x-axis remaining fixed and undistorted; d) the $x = 0$ surface (y-axis) having no restraints; and e) the bending of the beam due to the temperature distribution

$$T_x = a + bx^2 + cx^4 \tag{6}$$

The other beam is described in a similar fashion: a) the x-y axis intersect is held fixed; b) free expansion is allowed parallel and along the y-axis; c) the y-axis remains fixed and undistorted; d) the $y = 0$ surface (x-axis) has no restraints; and e) the bending of the beam due to the temperature distribution

$$T_y = d + e \cos \frac{\pi y}{1.3} \tag{7}$$

These two beams are shown in Figs. 7a and 7b, respectively. Both analytical and graphical solutions are available from elementary elasticity[10] for the determination of stress distributions and loadings on fixed end beams.

It can be seen in Fig. 7 that the greatly exaggerated distortion of the plate quadrant approximately follows the distortions caused by the two temperature distributions, Eq. (6) and (7). It is then apparent that the temperature induced bending of the two beams (Figs. 7a and 7b) is compensating. The compensating bending of the two beams is the basis for the following approximate semi-graphical solution of the stress distribution in the center area of the plate (Fig. 1).

Figure 18 is a typical representation of a number of figures showing the temperature distributions of the plate quadrant. On these figures the curves are approximated by linear temperature distributions

which are used to calculate the bending of the fixed end beams. The X-direction temperature distribution, T_x, given by Eq. (6) is used for obtaining the bending of the Y-direction beam and the Y-direction temperature distribution, T_y, given by Eq. (7) is used for obtaining the bending of the X-direction beam. Using the linear temperature approximations to find the bending of the beams does not impair the accuracy of the solution since the displacements average out as straight lines. Even though the displacement averages out, the temperature distribution T_x results in a stress distribution σ_y for the Y-direction beam and the temperature distribution T_y results in a stress distribution σ_x for the X-direction beam.

The solution for the two above cases is given by Timoshenko.[7] The solution leads to the following expressions for the stresses in the beams:

Y-direction beam

$$\sigma_y = \frac{1}{1-\nu}\left[-\alpha E T_x + \frac{1}{j}\int_{-j/2}^{j/2} \alpha E T_x \, ds + \frac{12s}{j^3}\int_{-j/2}^{j/2} \alpha E T_x \, s \, ds\right] \quad (14)$$

X-direction beam

$$\sigma_x = \frac{1}{1-\nu}\left[-\alpha E T_y + \frac{1}{k}\int_{-k/2}^{k/2} \alpha E T_y \, dr + \frac{12r}{k^3}\int_{-k/2}^{k/2} \alpha E T_y \, r \, dr\right] \quad (15)$$

where j and k are quadrant length and width, respectively, and

$$r = x - \frac{j}{2} \qquad dr = dx \quad (16)$$

$$s = y - \frac{k}{2} \qquad ds = dy \quad (17)$$

Obviously, the solutions are not correct at the ends of the beams, since

the stresses do not vanish there. However, at $y = 0$ for the Y-direction beam and $x = 0$ for the X-direction beam the stresses calculated will be correct to a high order of magnitude. As noted in the previous section with Eqn's (10) to (12), the Eqn's (14) and (15) also take into account the variation of properties with temperature. Using the argument of the previous section, the product αE is assumed constant, even though the error introduced is larger, but not in excess of ± 5 per cent. For each specific value of time the average of αE is used in the calculations.

The plate area of interest includes the x- and y-axis intersect. For this reason stress distributions are calculated based upon a) the temperature distribution T_x, at $y = 0$ for σ_y and b) T_y, at $x = 0$ for σ_x. These stress distributions are assumed to be correct over the center area of the plate.

Using Fig. 18 and its companion graphs as well as the linear temperature approximations, the bending of the two beams can be calculated. This is accomplished by dividing the beam into sections, and for each section finding the average of its two surface temperatures (based upon linear approximations). Then the expansions for these two temperatures are read from Fig. 21, and their difference represents the net expansion. From geometrical considerations the net expansion for each section is added to give the deflection for the beam.[10] This deflection corresponds to the r'-axis for the Y-direction beam and to the s'-axis for the X-direction beam, as shown in Figs. 7a and 7b. The variation in the coefficient of thermal expansion is included in the deflection and representative calculations are shown in Appendix B.

With deflections of the r'- and s'-axes known for the two beams, each beam is then analyzed as a simple fixed elastic beam by the

conjugate beam method.[10] With the deflection known the procedure is: a) successively differentiate the deflection twice; b) divide through by the product of the modulus of elasticity and the moment of inertia to find the moment at the ends; and c) differentiate twice more to obtain the loading on the beam.

Results of this procedure are shown in the sample calculations in Appendix B. From the calculations for the deflection curves r' and s' (Figs. 7a and 7b) the slopes of the respective curves can be plotted. The plot of values representing the differentiated slopes results in M/EI-diagrams for these elastic beams which represent plate quadrants.

For the Y-direction beam

$$I = \frac{j^3}{12} \tag{18}$$

and for the X-direction beam

$$I = \frac{k^3}{12} \tag{19}$$

The modulus of elasticity E is taken as a function of the temperature in the direction of the beam with average temperatures through the beam thickness being considered. With EI known, the moment diagram can be calculated and plotted.

These moment diagrams are an equivalence to the action due to temperature distributions in the beam causing the deflections of the r'- and s'-axis, respectively. It can be seen from Fig. 6 that the two beams have compensating bending and that the r- and r' axis as well as the s- and s' axis need not be parallel, and it is assumed that the moment diagrams compensate each other. It should be mentioned again that

the boundary conditions on the plate quadrant restrict the application of moments to the surfaces $y = 0$, $x = 0$. The averages of the moments are then taken for $y = 0$ in the y-direction beam and for $x = 0$ in the x-direction beam. These averages represent new zero references for the moment diagrams. With the moments at $x = 0$, $y = 0$ known, the resulting stresses on these surfaces are found from

$$\sigma_{max} = \frac{M c'}{I} \tag{20}$$

where c' represents either $j/2$ or $k/2$ as the half thicknesses of the beams.

The moment diagrams indicate that the boundary conditions, specifically zero moments at the surfaces $x = j$ and $y = k$ are not maintained. However, end effects such as yielding would change the moment at these edges. Since they are unknown, and since the interest is mostly at $x = 0$ and $y = 0$, the loading on the beams is found by differentiation over half the length. The loading condition thus obtained should theoretically be applied along the r'-axis and s'-axis for the Y-direction beam and X-direction beam, respectively. Since this is physically impossible, the loadings are assumed to apply along the surfaces $x = 0$ and $y = 0$.

With the known loadings on the surfaces, described by the coordinates $x = 0$ and $y = 0$, by superposition the resultant stress distribution can be obtained. For determination of strains it is assumed that the stresses in the area covered by the optical gage are identical wo the ones at $x = 0$ and $y = 0$ in the quadrants. Therefore the stresses σ_y on the surface $y = 0$ are constant between $y = \pm 0.172"$ and the stresses σ_x on the surface $x = 0$ are constant

between $x = \pm 0.500"$. The resultant strain from these stress distributions is then found from

$$\epsilon_x = \frac{1}{E} (\bar{\sigma}_x - \epsilon \bar{\sigma}_y) \quad , \tag{21}$$

where $\bar{\sigma}_x$ and $\bar{\sigma}_y$ are average stress values and E is a function of the average temperature.

III. EXPERIMENTAL TECHNIQUE

The objectives of the experimental program were the determination of transient thermal strains and temperature distributions in a Type 304 stainless steel plate heated to approximately 2000° F. The plate specimens were subjected to transient convective heating from an oxyacetylene flame.

A. Test Specimen

The selection of Type 304 stainless steel as a test material was made because of its low conductivity (approximately 10 Btu/hr/ft/°F) and its high coefficient of thermal expansion (11 x 10^{-6} inch/inch/°F). The physical and mechanical properties are readily available, and are shown in Appendix A.

The 0.240 x 2-1/4 x 4 inches specimens were made from 1/4" x 2-1/2" annealed bar stock and the final size was selected in accordance with available space in the test chamber which is referred to as the stagnation chamber. The specimens having the configuration shown in Fig. 1 were divided into two groups. One group had V-grooves on the specimens for location of the contact edges of the Tuckerman optical gage. The other group was used for temperature measurements and the specimens contained 1/8 inch diameter holes in locations as shown in Fig. 1. These holes were drilled to depths of 0.050, 0.075, 0.100, 0.150, and 0.200 inch from the heated surface to accommodate the thermocouples.

B. Heating Apparatus

The heating apparatus for this experimental program was developed previously and has been described in detail.[1,2,12,13,14] In former research programs the hot gases were directed parallel to the

surface of the test specimen. In this program the test plate is perpendicular to the flow of the hot gases, giving a stagnation heat input to the plate. The reasons for the change to the new test set-up were to obtain higher heat input, as well as uniform, symmetrical temperature distributions within the specimen.

The heating apparatus and its heating characteristics have already been described in detail.[12,13] Except for the test section, the apparatus remains unchanged, and will only be mentioned briefly. Basically the equipment consists of the oxygen and acetylene fuel sources, the lines and regulators, and the multiple nozzle flame head. The flame head consists of thirty separate nozzles arranged in a rectangle approximately 1" x 3-1/4".

For this investigation a "stagnation chamber" was built to hold the test specimen and direct the hot gases. The chamber, shown in Figs. 3 and 5, was lined on the sides, top and bottom, with 1/4" plates of commercial graphite and commercial refractory brick as a backing. The refractory brick served as an insulator for the steel shell of the chamber. The hot exhaust gases leaving the stagnation chamber were directed by exhaust ducts to be dispersed harmlessly.

The stagnation chamber was designed to expose a 4" x 1-3/4" area of the test specimen to the hot gases. The heat input to a test specimen was determined by using a molybdenum calorimeter plate technique.[13] The resulting heat flux for the x-y-z axis intersect of the test specimen as a function of temperature is shown in Fig. 8.

C. Preliminary Development of Technique for Transient Strain Measurements to 2000° F

This investigation was undertaken with the primary purpose of developing an experimental technique to extend the feasible temperature limit for measuring transient strains. Two techniques were studied which have practical limits near 1500° F, the electric-resistance foil gage and the Tuckerman optical strain gage.

Potentially, the Tuckerman optical strain gage offered more advantages than the electric-resistance foil gage, and was finally selected for the experimental program.[2] The Tuckerman optical strain gage system consists of two basic units, the autocollimator and the extensometer. To adapt the gage to measure the transient strains while the specimen is reaching a temperature of over 2000° F required modification of the gage and the design of a protective heat shield to prevent heat transfer into the gage.

To keep the specimen in position and at the same time allow for free expansion, a holding device was constructed. This device had the added advantage of preventing vibration of the specimen, and subsequently gave more reliable strain measurement data.

1. The Tuckerman Optical Strain Gage

The development of the Tuckerman optical strain gage dates back four decades.[24] Recent refinements have made possible the measurement of strains in tension and compression as small as 0.000002 inch/inch on metals and other materials. This precision and adaptability ideally suit the measurement of thermal strains.

The extensometer and the autocollimator are the two basic units of the system. The extensometer consists of the gage body, the

rotating lozenge, and the fixed knife edge, which are constructed of cold-rolled steel, Stellite (an alloy steel), and hardened carbon steel, respectively. One surface of the rotating knife edge or lozenge is ground, lapped, and polished to an optically flat mirror. The lozenge is connected to the gage body by special springs and clips which hold it in light contact with the gage without restraining its movement. Deformation of the specimen causes the lozenge to rotate. The autocollimator is a precision telescope consisting of a highly corrected objective lens system, a reticle consisting of a fiducial spot and scale, a light source illuminating the fiducial mark, and an eyepiece.[15]

A schematic diagram[16] illustrates the principle by which the autocollimator and extensometer function. Deformation of the specimen causes the lozenge to rotate and move the fiducial spot across the scale. The maximum range of readings obtainable (in terms of the scale) is from 0 to 60, with a least count of 0.02. A simple formula converts the readings to strain values.

The extensometer used in the tests had a 1-inch gage length and a 0.4-inch lozenge. The least count of the vernier scale readings is 8 microinches per inch. This optical strain gage was designed primarily for static strain measurements at steady state temperatures, and has a recommended maximum operating temperature of 500° F.[15] The limiting condition is excessive heating of the mirrored surface of the lozenge. It was assumed that by modifying the extensometer to prevent a large temperature rise its accuracy would not be impaired and its versatility would be greatly increased.

2. Extensometer Modifications

The prevention of heat conduction from the specimen plate into the extensometer body was accomplished by the attachment of heat sinks to the knife edge and lozenge. These heat sinks consisted of the flow of water through two 1/16" diameter copper tubes attached to the knife edge and two 1/16" diameter copper tubes attached to the lozenge. The combined water flow rate was maintained at approximately 4 pounds per minute.

The attachment of the copper tubing to the knife edge and lozenge was complicated by the extreme hardness of the steel of which the knife edge and lozenge are made. The knife edge and lozenge were manufactured from hardened carbon steel and Stellite, respectively. The hardness of these two materials necessitated that the grooves for the tubing be ground by a 1/16" width grinding wheel. The copper tubing was fastened to the knife edge and lozenge by soft solder. This arrangement is shown in Figs. 2 and 5.

3. Heat Shield

The radiant heat shield shown in Fig. 3 consists of copper tubing, through which water flows, attached to a copper plate. The depth of the shield was limited by the clearance (0.22") between the extensometer body and the surface of the specimen. To provide this clearance the heat shield was designed with a depth of 0.015". To present a uniform heat sink surface to the specimen the overall dimensions of the heat shield were 3" x 4-1/2", which is larger than the 2-1/2" x 4" specimen plate. Grooves were milled through the plate for the knife edge and lozenge of the extensometer.

4. Specimen Holding Device

The specimen holding device prevented external constraint as the test plate expanded with increasing temperature within the stagnation chamber. Also, this holding device helped to eliminate vibration of the specimen and thereby increased the reliability of the strain readings.

The stainless steel holding device kept the specimen plate in position with six 1/32" diameter tungsten pins, two pins at each of the three locations shown in Fig. 1. The pins were free to change position as the plate expanded. Tungsten was selected as the pin material because of its high melting point and relatively high strength at high temperatures.

D. Test procedure and Technique for Strain Measurements

Before tests were undertaken it was expected that visual readings of the autocollimator scale might not be feasible. This was realized with occurrence of a large rate of change of scale readings (approximating 20,000 microinches in 90 seconds). Since the strain deformation was given by a light spot moving across a dark scale, a film recording using a movie camera was selected as a recording method.

A Bolex H16, 16 mm movie camera was used for recording strain readings. To photograph the scale the eyepiece of the autocollimator was removed. The camera lens system required was a 50 mm magnifying lens on a 35 mm extension tube. A camera drive was obtained which gave the camera a frame speed of about 30 frames per second.

The film requirement of the camera was determined by preliminary recordings of the light spot on the scale of the autocollimator.

Initially Kodak Tri-X film was used, but when developed it was found to be blank. Apparently more sensitive film was needed for recording the light spot, and Kodak Royal Pan X, which has a sensitivity rating of 1200 ASA was obtained. Careful film development resulted in very satisfactory pictures of the light spot.

From previous tests[2] it was known that any heating of the extensometer resulted in a systematic error in the strain readings. This error was introduced by the thermal expansion of the extensometer, and was registered as an apparent compressive strain. To determine the correction for this effect, the thermal expansion of the extensometer was calibrated. This calibration[2] showed that the average thermal expansion coefficient was 7.30 microinches per inch per degree Fahrenheit.

The heat shield and copper tubing attached to the knife edge and lozenge were highly effective in keeping the temperature rise in the extensometer to a minimum. For each of the strain measurement tests two thermocouples were attached to the extensometer. The maximum temperature rise was less than 25° F, and the maximum temperature difference between the two thermocouples was less than 3° F.

To keep a record of the reproducibility of each test, a control thermocouple was placed against the back surface of the specimen. It was known[1,2] that a variation in temperature distributions could be expected and that a subsequent variation in strain measurements from test to test would be likely. This variation results from the change in the flow rate of the gases into the test chamber.

The procedure followed for setting up each test was the same. The plate was held in position in the stagnation chamber by the specimen

holding device. The heat shield was placed against the unheated surface of the specimen plate with a 1/32" gap maintained by placing 1/32" diameter wires at the four corners of the plate. As shown in Fig. 4, the extensometer, instrumented with two thermocouples, was placed (with the two knife edges in the grooves of the heat shield) against the plate and held in position by two spring-tensioned wires. It was then necessary to shift the extensometer knife edges until they were fitted into the V-grooves on the specimen. A thermocouple was placed against the back surface of the plate, and the outputs of the three thermocouples were recorded on a 12-channel Minneapolis-Honeywell recording oscillograph. The autocollimator was aligned and adjusted with the extensometer, after which the cooling water for the extensometer and heat shield was turned on. The camera was loaded with film and aligned.

To obtain a record of the beginning and end of each test an electric switch was fastened to the valve which controls the flow of gases into the test chamber. This switch started and stopped the camera and its action was also recorded on the oscillograph. The exact count of the film frames used during each tests was obtained with a mirror to overexpose the film before and after each tests. Each test began with the ignition of the oxyacetylene flame, and the specimens were heated for about 90 seconds. After completion of each test the autocollimator was checked to see if the light spot remained on the scale. Useful data were obtained for six experimental tests.

The pilot tests did not yield strain data, but showed that the test set-up, extensometer modifications, and heat shield performed as expected.

From the developed film of each test the scale readings were reduced, frame by frame. Although the vernier scale of the light spot was difficult to interpret, each reading for the plotting of the strain curve averaged out and the results are within an accuracy of ± 20 micro-inches.

E. Technique and Test Procedure for Temperature Measurements

Since the technique for measuring transient temperature distributions in a flat plate has already been described,[1] it will be briefly outlined. The technique consists of insertion of thermocouples into 1/2" diameter flat-bottomed holes milled in the specimen. The thermocouples, contined in 3/32" diameter, two-hole ceramic tubes, were spring-loaded into the locations shown in Fig. 1, and the general arrangement is shown in Fig. 5. Number 32 gauge chromel-alumel thermocouples were used and a continuous record of their output was obtained on the Minneapolis-Honeywell recording oscillograph. Temperatures were recorded at depths of 0.240", 0.200", 0.150", 0.100", 0.075", and 0.050" from the heated surface.

IV. EXPERIMENTAL RESULTS

The experimental results consist of the strain measurements on the unheated surface of the specimens and the temperature distributions within the plate specimens.

The optical strain measurements as a function of time are shown in Fig. 9. The curves show the continuous camera recording of the strain at the center of the unheated surface. The values in Fig. 9 have been corrected to account for the thermal expansion of the extensometer. Test data for experimental runs where an obvious knife edge displacement occurred or which were prematurely terminated have not been included in the graph of Fig. 9. The variation in data between the individual tests is consistent with the temperature distributions within the plate specimens. The temperatures of the unheated surface as measured by a control thermocouple at $x = 25/32$ inches and $y = 11/16$ inches are shown in Fig. 10. It was found previously[1] that from test to test variations of $\pm$ 6 per cent exist in temperature measurements. In Fig. 10 the temperature curve of Test 9 is probably incorrect, having a considerably larger variation than the remaining curves. For the purpose of comparing the experimental strain results with the semianalytical solution, the mean average of the data is shown in Fig. 11.

The continuous temperature records obtained on the oscillograph were plotted as functions of time at various depths below the heated surface. A typical curve is shown in Fig. 14 for temperatures at the specimen location $x = 1\text{-}25/32$ inches, $y = 0$. Figure 15 shows a cross plot of these temperatures vs. depth below the heated surface at various times. The typical cross plot in Fig. 15 is for the location $s = y = 0$, and is the only one of its type required for the calculation of the

thermal stress distributions and strains. The approximate temperature curves T_z for the points are shown on this figure as solid lines. The slope of the curves at the heated surface was determined from the conductivity of the stainless steel and from the heat flux into the plate, since it was obvious that the temperature records indicated too high an initial slope.

The cross-plots shown in Figs. 15 and 16 represent the temperature distributions on the unheated surface of the plate for the respective x and y-axes at various times. The points shown are the unheated surface intercepts of the temperature distributions through the thickness. The curves T_x and T_y drawn through the points are represented by solid lines, and were required for the calculation of the thermal stress distributions and the strains.

With the fitted curves of Figs. 15, 16, and 17 known, it is possible to combine Eqn's (6), (7), and (8), resulting in Eq. (5)

$$T(x,y,z) = \frac{T_z}{a}(T_x-a) + \frac{T_z}{a}(T_y-a) + \frac{T_x T_y}{a^2}(T_z-a) + a \qquad (5)$$

where

$$T_x = a + bx^2 + cx^4 \qquad (6)$$

$$T_y = d + e\cos\frac{\pi y}{1.3} \qquad (7)$$

$$T_z = f + g(z+0.120) + h(z+0.120)^2 + i(z+0.120)^3 \qquad (8)$$

The symmetry of the x-y plane of the plate formed the basis for the semi-analytical determination of the strain. The temperature distributions of one plate quadrant for the unheated surface were obtained and a typical set of curves is shown in Fig. 18.

V. COMPARISON OF SEMI-ANALYTICAL AND EXPERIMENTAL STRAIN RESULTS

Before the semi-analytical and experimental strain results are compared, the semi-snalytical solution will be discussed. The temperature distributions expressed by Eq. (5) were used for determining the strain on the unheated surface of the plate. This strain was calculated for the same area over which the extensometer measured strain. To determine the strain over this area it was necessary to obtain the thermal stress distribution using an approximate method of analysis. The sequence used in the determination of the stress distributions assumed independent interaction of stresses which allowed the final result to be obtained by the method of superposition. Furthermore, the analysis assumed that there was no plastic deformation and that the basic relationships of elasticity and thermoelasticity applied throughout the plate.

The semi-analytical solution of the strain consists of two parts. In part I the strains are calculated from the stress-strain relationships, and are shown in Fig. 12. In part II the strains or thermal expansion values are obtained from the temperatures on the unheated surface of the specimen, and are shown in Fig. 13. An additional curve in Fig. 13 shows the combined results of parts I and II as the total calculated strain. The strain based on the free expansion as a result of temperature is subject to errors in temperature measurements, and is therefore subject to the deviation of true thermal expansion as compared to the linear thermal expansion curve shown in Fig. 21.

Referring again to Fig. 12, it is noted that the curve representing the results of stress-strain calculations was calculated with the assumption that plastic deformation did not exist within the plate. However, the sample calculations show that unknown boundary conditions

at the plate edges result in negligible plastic deformation and no large errors are introduced with the assumption of a perfectly elastic body.

In Fig. 11 the results of the semi-analytical strain calculations are compared with the strain measurements. The strain measurement curve represents the average of the experimental curves, and it can be noted that good agreement exists until approximately 60 seconds have elapsed. At that time the divergence of the curves begins and becomes increasingly larger as time goes on.

One explanation for the divergence could be the partially plastic behavior of the plate. As shown in Fig. 23, the yield strength above 1500° F would be too low for maintaining the elastic character of the specimen, thereby making it impossible to determine strains within the plate. Another reason for the divergence could be the influence of the heat conducted through the extensometer knife edges on the plate temperature distribution. The heat conduction through the points of contact of the extensometer was not expected to influence to any extent the strain calculations, since the large temperature gradients at those points would result in localized yielding. Since the divergence of the two strain curves indicated that this influence could not be ignored, a check was made on the local temperature distribution for heat conduction through the contact edge of the lozenge. By assuming that steady state conditions were reached in the plate, an approximate temperature distribution using the known geometry of the plate and extensometer[11] was determined by a flux plot. This flux plot for the lozenge is shown in Fig. 19. It is apparent from this flux plot that with the heated surface of the plate near 2000° F the temperature distribution in the vicinity of the contact edges of the lozenge was greatly changed from the assumed

temperature distribution used in the semi-analytical calculations. Since yielding took place in the plate near the contact edge of the extensometer, it was not possible to determine a correction for either of the strain results.

Partial elimination of the divergence of the strain results at high temperatures could best be done by increasing the heat flux into the plate or by decreasing the thermal conductivity of the lozenge and knife edge material of the extensometer.

VI. CONCLUSIONS AND RECOMMENDATIONS

For the material and geometry of the specimen under the described test conditions, the following conclusions are reached:

1. A solution was obtained for the transient strain variation on the unheated surface of a homogeneous flat Type 304 stainless steel plate exposed to a non-uniform heating rate distribution on one surface. The solution is presented for a particular three-dimensional temperature distribution in a flat plate at the center area of the unheated surface.
2. An experimental technique was developed which measures transient thermal strains up to 2000° F using a modified Tuckerman optical strain gage.
3. The strains measured in heated Type 304 stainless steel were in good agreement with the strains calculated from the analytical solution.
4. Comparison of experimental and calculated strains show that for annealed Type 304 stainless steel the properties presented in Appendix A and used in the calculations are valid within small errors of less than 5 per cent.

The experimental technique for measuring strains could be extended to cover materials several hundred degrees Fahrenheit above 2000° F if the following recommendations were carried out:

1. Construct the knife edges of the extensometer from a material of low thermal conductivity which can withstand very high temperatures, such as a diamond-ceramic combination.

2. Construct the radiation heat shield with the surface facing the heated specimen coated with a highly reflective substance.
3. Construct the extensometer body from a material with a low coefficient of thermal expansion.

BIBLIOGRAPHY

1. D. R. Hornbaker, "Transient Temperature Distributions in a Thermally Orthotropic Plate with Non-Uniform Surface Heating," Univ. of Calif. Eng. Proj. Report HE-150-189, June 1961.
2. B. H. Suzuki, "Thermal Stress-Strain Distribution in a Transversely Anisotropic Material During Transiwnt Heating," Univ. of Calif. Eng. Proj. Report HE-150-196, March 1962.
3. P. J. Schneider, "Variation of Maximum Thermal Stresses in Free Plates," J. Aero. Sci. 22, 12, 872, 1955.
4. B. E. Gatewood, "Thermal Stresses in Moderately Thick Elastic Plates," J. Appl. Mech. 432-436, September 1959.
5. B. E. Gatewood, Thermal Stresses, McGraw-Hill Book Company, Inc., New York, 1957.
6. B. A. Boley, J. H. Weiner, Theory of Thermal Stresses, John Wiley and Sons, Inc., New York, 1960.
7. S. Timoshenko, J.N.Goodier, Theory of Elasticity, 2nd Ed., McGraw-Hill Book Co., New York, 1951.
8. H. B. Callen, Thermodynamics, John Wiley and Sons, Inc., New York, 1960.
9. I. S. Sokolnikoff, Mathematical Theory of Elasticity, 2nd Ed., McGraw-Hill Book Co., New York, 1956.
10. E. P. Popov, Mechanics of Materials, Prentice-Hall, Inc., Englewood Cliffs, N.J., 1952.
11. W. H. Giedt, Principles of Engineering Heat Transfer, Van Nostrand, Princeton, N. J., 1957.
12. D. Wizansky, E. J. Russ, "An Oxyacetylene Flame Apparatus for Surface Ablation Studies," Univ. of Calif. Eng. Proj. Report HE-150-167, January 1959.

13. E. J. Russ, "Heating Rate Characteristics of an Oxyacetylene Flame Apparatus for Surface Ablation Studies," Univ. of Calif. Eng. Proj. Report HE-150-176, December 1960.

14. L. L. Cobb, Jr., "The Influence of Hydrogen Recombination on Turbulent Flow Heat Transfer to a Flat Plate," Univ. of Calif. Eng. Proj. Report HE-150-183, June 1960.

15. "Optical Strain Gage," American Instrument Co., Inc. Bulletin 2294, July 1959.

16. H. D. Howerton, "Optical Strain Gages for Use at Elevated Temperatures," ASTM, Spec. Tech. Pub. No. 230, 1958.

17. R. V. Melette, Thermal Stresses in Thin Rectangular Plates, Univ. of California at Berkeley Master's Thesis, 1956.

18. C. W. Muhlenbruch, V. N. Krivobok, C. R. Mayne, "Mechanical Properties in Torsion and Poisson's Ratio for Certain Stainless Steel Alloys," ASTM Authorized Reprint, Volume 51, 1951.

19. D. E. Furman, "Thermal Expansion Characteristics of Stainless Steels Between -300° and 1000° F," Journal of Metals, April 1960.

20. Stainless Steel Handbook, Allegheny Ludlum Steel Corp., Pittsburgh, Pa., 1956.

21. Strength of Metal Aircraft Elements, Military Handbook ANC-5 Bulletin, Armed Forces Supply Suport Center, Washington 25, D.C., March 1955.

22. H. Dunegan, "Dynamic Modulus of 304 Stainless Steel as a Function of Temperature," (Special Report), Lawrence Radiation Lab., Livermore, Calif., June 1962.

23. Thermophysical Properties of Solid Materials, Vol. 11 - Alloys, Armour Research Foundation, Revised Ed., November 1960.

24. L. B. Tuckerman, "Optical Strain Gages and Extensometers," ASTM, Vol. 23, 1923.

25. ASM Metals Handbook, 1960 Edition.

APPENDIX A

A. PROPERTIES OF TYPE 304 STAINLESS STEEL

Extensive data are available on the properties and composition of Type 304 stainless steel. Among the several references available for these properties there is as much as a 10 per cent variation in the values of the respective properties. The properties quoted here and used in the calculations are the best available.

The composition[20] of Type 304 stainless steel is:

Element	Per cent
Carbon	0.08 max.
Manganese	2.00 max.
Silicon	1.00 max.
Chromium	18.00 - 20.00
Nickel	8.00 - 11.00
Iron	the rest

The data on the modulus of elasticity[22] are shown plotted against temperature in Fig. 20.

The thermal expansion of Type 304 stainless steel is plotted against temperature in Fig. 21, and represents[23] a median curve for data points obtained by several investigators for alloy compositions of 16 - 19 per cent Chromium and 7 - 16 per cent Nickel. The curve was differentiated to obtain the coefficient of thermal expansion shown plotted versus temperature in Fig. 22.

The yield strength in tension[21] is plotted against temperature in Fig. 23.

For Poisson's ratio no data were available on the variation with temperature, and it is assumed constant[18] and equal to 0.305.

The thermal conductivity[25] is plotted vs. temperature in Fig. 24.

APPENDIX B

B. CALCULATION OF STRESSES

B.1 Stress Calculations for Temperature Distribution, T_z

The stress distribution in the plate resulting from the temperature distribution, Eq. (9), is given by Eqn's (10), (11), and (12). Substituting Eqn's (11) and (12) into Eq. (10) gives

$$\sigma_x = \sigma_y = \frac{\alpha E}{1-\nu} \left[- T_z + \frac{1}{2p} \int_{-p}^{p} T_z \, dz + \frac{3z}{2t^3} \int_{-p}^{p} T_z \, z \, dz \right] \qquad (1\text{-A})$$

By substitution of Eq. (9) and $q = z + p$

$dq = dz$

Equation (1-A) becomes

$$\sigma_x = \sigma_y = \frac{\alpha E}{1-\nu} \left\{ - f - gq - hq^2 - iq^2 + \frac{1}{2p} \int_{o}^{2p} (f + gq + hq^2 + iq^3) \, dq \right.$$

$$\left. + \frac{3(q-p)}{2p^3} \int_{o}^{2p} [f + gq + hq^2 + iq^3] \, (q-p) \, dq \right\} \qquad (1\text{-B})$$

Integrating and substituting $p = 0.120"$

$$\sigma_x = \sigma_y = \frac{\alpha E}{1-\nu} \left[- hq^2 - iq^3 - 0.009600 \, h - 0.0002765 \, i \right.$$

$$\left. + 0.2400 \, hq + 0.05184 \, iq \right] \quad \text{psi} \qquad (1\text{-C})$$

where α = the coefficient of expansion, evaluated at the average temperature through the thickness of the plate for the appropriate time

E = the modulus of elasticity, evaluated at the same average temperature

ν = Poisson's ratio (0.305)

q = 0.24" for the back surface of the plate

h and i = constants for the temperature curves in Fig. 15.

The numerical calculations are shown for a time parameter of 40 seconds.

To evaluate Eq. (1-C), the following values are determined:

with $T_z = 1277 - 1300\ q + 2400\ q^2$ °F

the average temperature = 1205 °F

and $\alpha = 12.48 \times 10^{-6}$ in/in/°F

$E = 20.0 \times 10^6$ psi

Substituting the above values for α and E and $\nu = 0.305$, $h = 2400$, and $i = 0$ into Eq. (1-C), the result is

$$\sigma_x = \sigma_y = 359\ (-\ 2400\ q^2 - 23.04 + 5679)\ \text{psi} \qquad (1\text{-D})$$

For the back surface of the plate ($q = 0.240"$) at $x = y = 0$

$$\sigma_x = \sigma_y = -\ 8{,}280 \quad \text{psi}$$

To show the stress dependence on the temperature distribution T_z, stresses are calculated for $q = 0$ to $q = 0.240"$, and are shown in Fig. 26.

B.2 Stress Calculations in the y-direction Beam at $y = 0$ for Temperature Distribution, T_x

This section of the sample calculations determines the stress, σ_y, given by Eq. (14), that is dependent upon the temperature distribution, T_x (Eq. (6)). Substituting Eq. (6), $s = s - \frac{j}{2}$, and $ds = dx$ into Eq. (14), σ_y becomes

$$\sigma_y = \frac{\alpha E}{1-\nu}\left[-\ a - bx^2 - cx^4 + \frac{1}{j}\int_0^j (a + bx^2 + cx^4)\ dx + \frac{12(x - \frac{j}{2})}{j^3}\right.$$
$$\left.\int_0^j (a + bx^2 + cx^4)(x - \frac{j}{2})\ dx\right] \qquad (2\text{-A})$$

Integrating and substituting $j = 2"$

$$\sigma_y = \frac{\alpha E}{1-\nu} [- bx^2\ 2\ cx^4 + 2.000\ bx + 6.400\ cx - 0.667\ b - 3.200\ c]\ psi \quad (2\text{-B})$$

where α = the coefficient of thermal expansion, evaluated at the average temperature through the thickness of the plate for the appropriate time.

E = the modulus of elasticity, evaluated at the same average temperature

ν = Poisson's ratio (0.305)

b and c = constants for the temperature curves in Fig. 16.

As in the previous section, the numerical calculations are made for a time parameter of 40 seconds. To evaluate Eq. (2-B), the following values are determined:

with $T_x = 1103 + 35x^2 + 15x^4$ °F

the average temperature = 1239 °F

and $\alpha = 12.48 \times 10^{-6}$ in/in/°F

$E = 19.8 \times 10^6$ psi

Substituting the above values of α and E and $\nu = 0.305$, $b = 35$, and $c = 15$ into Eq. (2-B), the result is

$$\sigma_y = 357\ (- 35x^2 - 15x^4 + 166x - 71.33)\ psi \quad (2\text{-C})$$

Substituting values for x $(0 < x < 2")$ into Eq. (2-C) results in the stress distribution shown in Fig. 26.

B.3 Stress Calculations in the x-direction Beam at x = 0 for Temperature Distribution, T_y

The stress, σ_x, given by Eq. (15), is dependent upon the temperature distribution, T_x (Eq.(7)). Substituting Eq. (7), $r = y - \frac{k}{2}$, and $dr = dy$ into Eq. (14), the expression for σ_x is

$$\sigma_x = \frac{\alpha E}{1-\nu} \left[- d - e \cos \frac{\pi y}{1.3} + \frac{1}{k} \int_o^k (d + e \cos \frac{\pi y}{1.3}) \, dy + \frac{12(y - \frac{k}{2})}{k^3} \right.$$

$$\left. \int_o^k (d + e \cos \frac{\pi y}{1.3})(y - \frac{k}{2}) \, dy \right] \qquad (3\text{-A})$$

Integrating and substituting $k = 1.125"$

$$\sigma_x = \frac{\alpha E}{1-\nu} e \, (- \cos \frac{\pi y}{1.3} - 1.9534 \, y + 1.2498) \quad \text{psi} \qquad (3\text{-B})$$

where α = the coefficient of thermal expansion evaluated at the average temperature through the thickness of the plate for the appropriate time.

E = the modulus of elasticity evaluated at the same average temperature

ν = Poisson's ratio (0.305)

e = constant for the temperature curves in Fig. 17.

The temperature curve at 40 seconds is used for the numerical calculations. From this temperature curve

$$T_y = 795 + 308 \cos \frac{\pi y}{1.3}$$

the following values are determined:

Average temperature = 840° F

and $\alpha = 11.82 \times 10^{-6}$ in/in/°F

$E = 22.9 \times 10^6$ psi

The above values for α and E, $\nu = 0.305$ and $e = 308$ are

substituted into Eq. (3-B). Then

$$\sigma_x = 120{,}000 \quad (- \cos \frac{\pi y}{1.3} - 1.9534\, y + 1.2998) \quad \text{psi} \qquad (3\text{-C})$$

After substituting values of y into the above equation the stress distribution shown in Fig. 27 is obtained.

B.4 Stress Distributions from Conjugate Beam Analysis

The linear temperature distributions typically shown in Fig. 18 are used to determine the deflection of the Y-direction and X-direction beams. The first step in finding the deflections is to divide the beams into sections. The Y-direction beam is divided into three segments, 0 to 0.4", 0.4" to 0.8", and 0.8" to 1.125". Likewise, the X-direction beam is divided into three segments, 0 to 1.0", 1.0" to 1.5", and 1.5" to 2.0". From Fig. 18 the linear temperature distributions are known at 0, 0.4", 0.8", and 1.125" for the Y-direction beam, and 0, 1.0", 1.5", and 2.0" for the X-direction beam. The average temperatures of the two beam surfaces are found for each of the segments. These average temperatures are then used to read the values of the expansions of each segment's two surfaces from Fig. 21. The expansion difference is divided by the beam depth and multiplied by the segment length. The result represents the change in slope of the beam segment's two ends in inches/inch. From the trigonometric identity that this change in slope of the two segment ends represents the change in slope of the deflection the curve representing the bending of the beams is constructed.

To show the above steps numerically the Y-direction beam deflection curve is constructed for the temperature distribution at 40 seconds.

Location (y)	Distribution °F	Surface Temperature for x=0 °F	Surface Temperature for x=2.0" °F	Average Surface Temperature for x=0 °F	Average Surface Temperature for x=2.0" °F
0	1050 - 165x	1050	1380		
0.2				982	1312
0.4	915 - 165x	915	1295		
0.6				762	1092
0.8	610 - 165x	610	940		
0.962				530	860
1.125	450 - 165x	450	780		

Segment Length Inches	Thermal Expansion for x=0 inches x 10^6	Thermal Expansion for x=2.0" inches x 10^6	Net Thermal Expansion inches x 10^6	Deflection Slope Change inches x 10^6/inch
0.4	9800	13,850	4,050	810
0.4	7200	11,100	3,900	780
0.325	4550	8,350	3,800	617

For the Y-direction beam at 40 seconds the following values of EI are used in the calculation:

Location (y-in)	0	0.2	0.4	0.6	0.8	0.962	1.125
Ave. Temp. °F	1215	1197	1070	927	775	705	615
E x 10^{-6} psi	19.9	20.5	21.1	22.2	23.4	24.0	24.7
EI x 10^{-6} $(in)^2$	13.27	13.68	14.08	14.80	15.60	16.0	16.48

With the magnitude of the moments known at $x = 0$ and $y = 0$ for the two beams, the stress distribution at these two ends (caused by the moments) can be calculated, using Eq. (20). The values of I for the beams were determined previously and are repeated: For the Y-direction beam $I = 0.667\ (in)^4$ and for the X-direction beam $I = 0.1186\ (in)^4$. The calculated values for the maximum stress at 40 seconds are:

Y-direction Beam

$$\sigma_{y_{max}} = \frac{M\,c'}{I} = \frac{3.770(1)}{0.667} = 5{,}650 \text{ psi}$$

X-direction Beam

$$\sigma_{x_{max}} = \frac{M\,c'}{I} = \frac{3{,}770\ (\frac{1.125}{2})}{0.1186} = 17{,}900 \text{ psi}$$

The final step in calculating the stress distributions σ_x and σ_y for the two beams is accomplished by twice differentiating the two moment diagrams.

By the principle of superposition the preceding separately calculated stresses are added and the plate quadrant has the stress distributions, σ_x at $x = 0$ and σ_y at $y = 0$, as shown in Figs. 28 and 29, respectively.

B.5 Calculated Strain at Gage Location on Specimen

The strain resulting from the stress distributions shown in Figs. 28 and 29 is calculated from Eq. (21),

$$\epsilon_x = \frac{1}{E}\ (\bar{\sigma}_x - \nu\,\bar{\sigma}_y) \qquad (21)$$

where $\bar{\sigma}_x$ and $\bar{\sigma}_y$ are the average stresses between the limits $-0.5" < x < 0.5"$ and $-0.172" < y < 0.172"$, respectively. E is determined from Fig. 20 with average temperatures within the above limits.

For the calculation of the strain at 40 seconds the following values are used:

$$\bar{\sigma}_x = 12{,}800 \text{ psi}, \quad \bar{\sigma}_y = 15{,}800 \text{ psi}, \quad E = 20.9 \times 10^6 \text{ psi}$$

After substitution of these values and $\nu = 0.305$ into Eq. (21), the resulting strain is found to be $\epsilon_x = 844 \times 10^{-6}$ in.

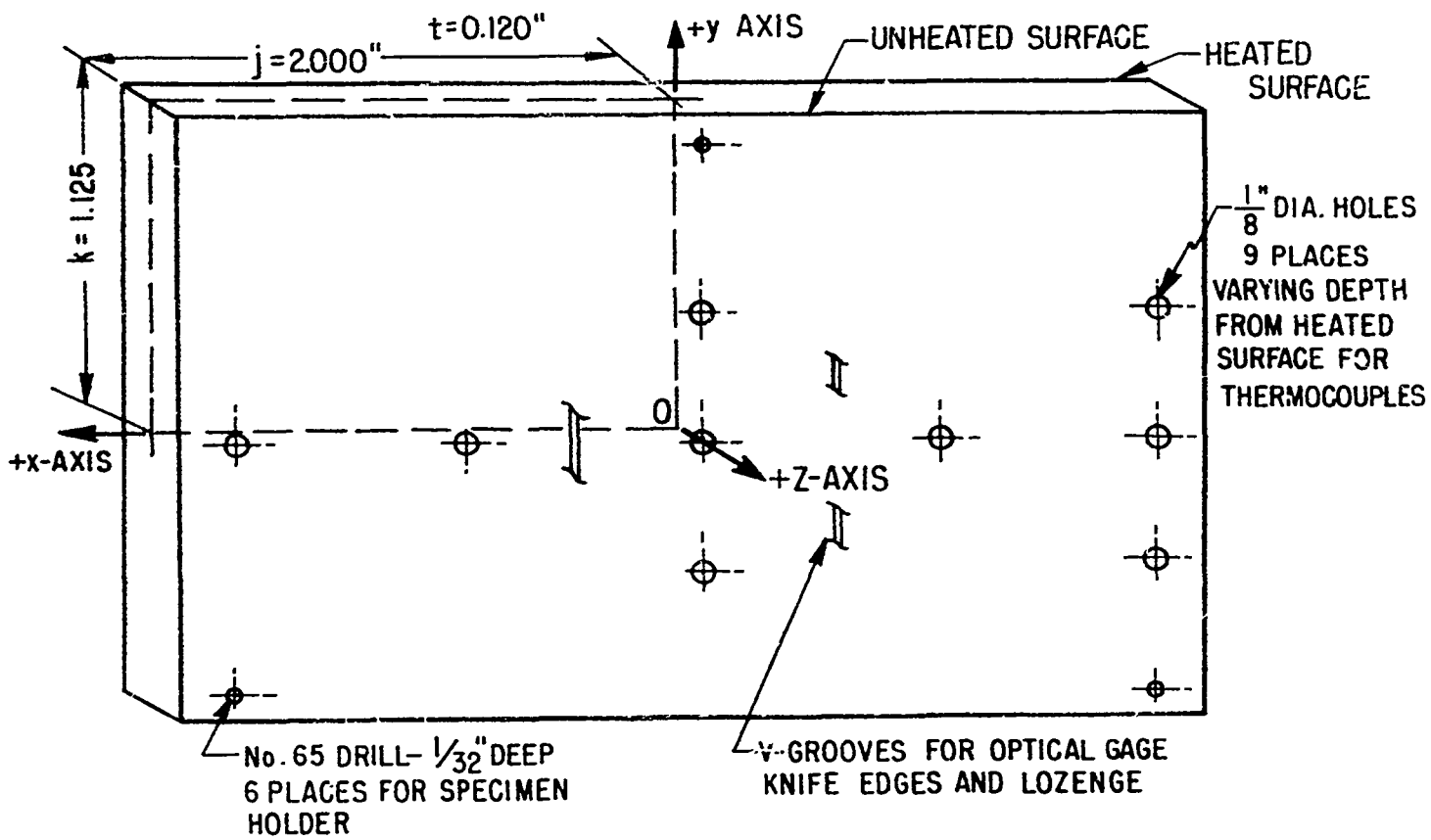

FIG. 1 SPECIMEN CONFIGURATION SHOWING THERMOCOUPLE AND STRAIN GAGE LOCATIONS

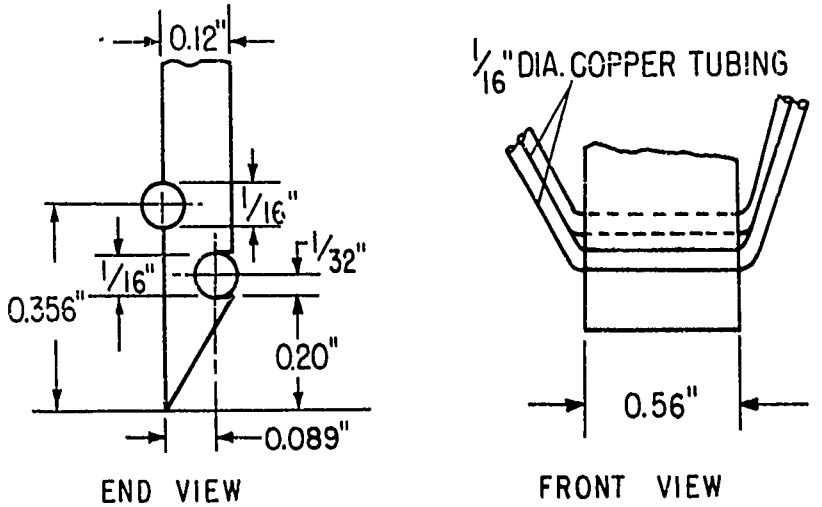

KNIFE EDGE

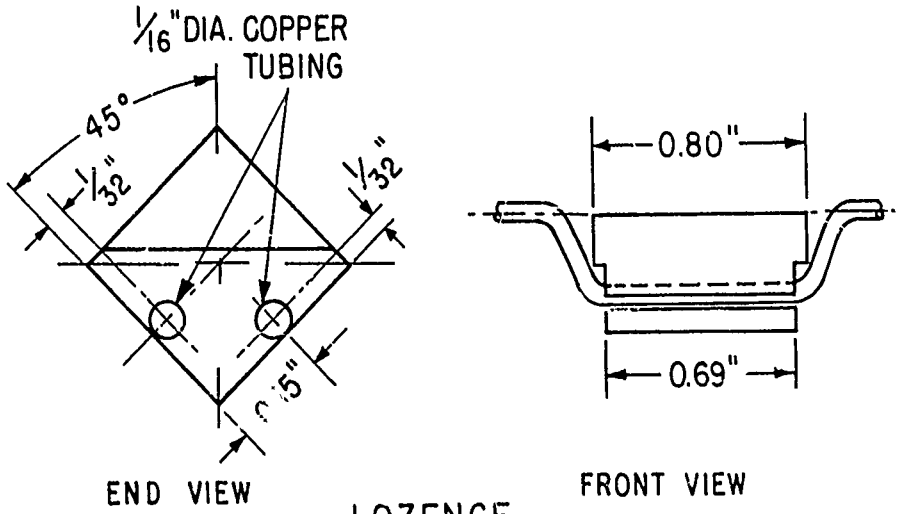

LOZENGE

FIG. 2 STRAIN GAGE MODIFICATIONS FOR COOLING OF KNIFE EDGE AND LOZENGE

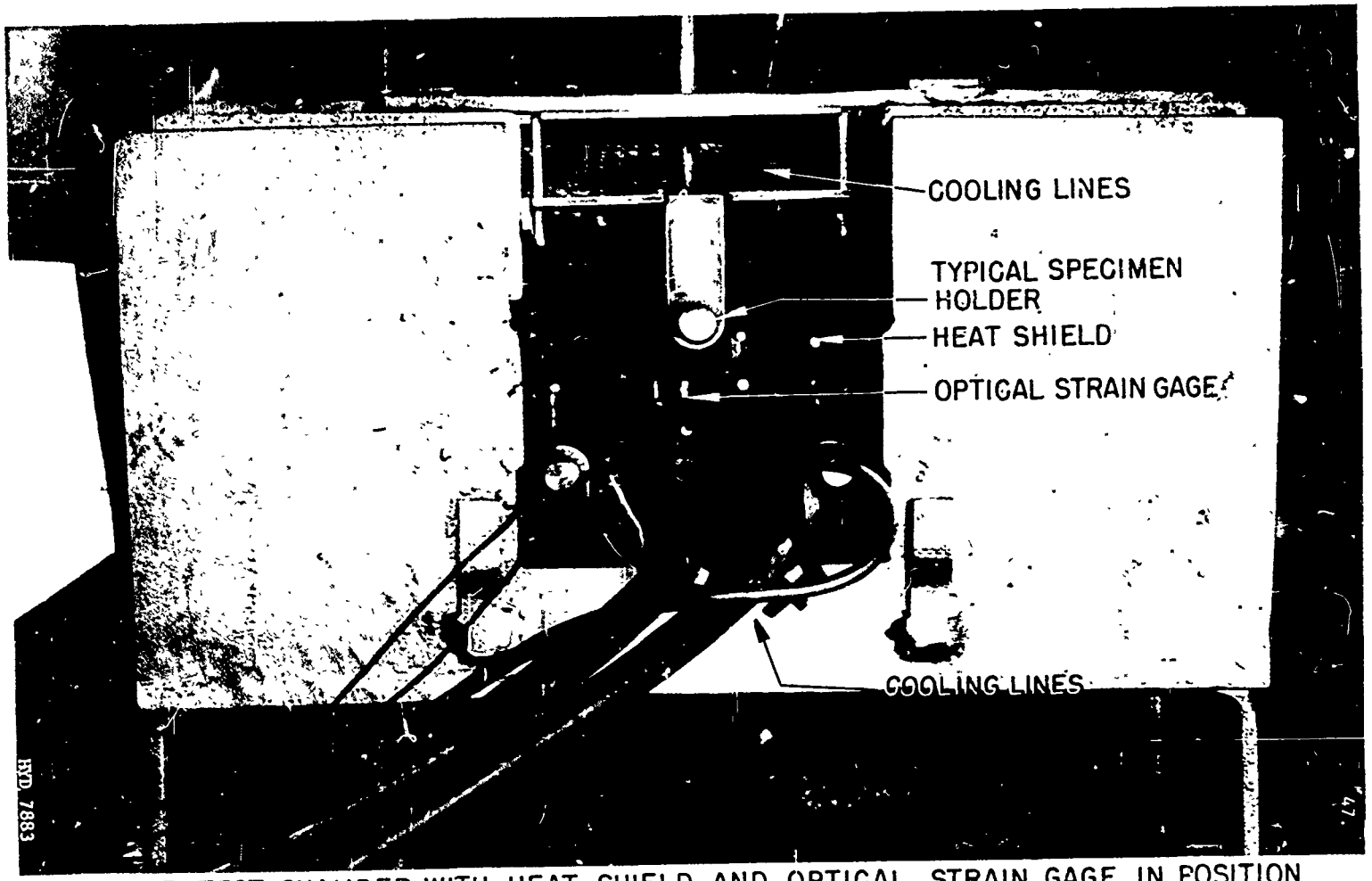

FIG.3 TEST CHAMBER WITH HEAT SHIELD AND OPTICAL STRAIN GAGE IN POSITION

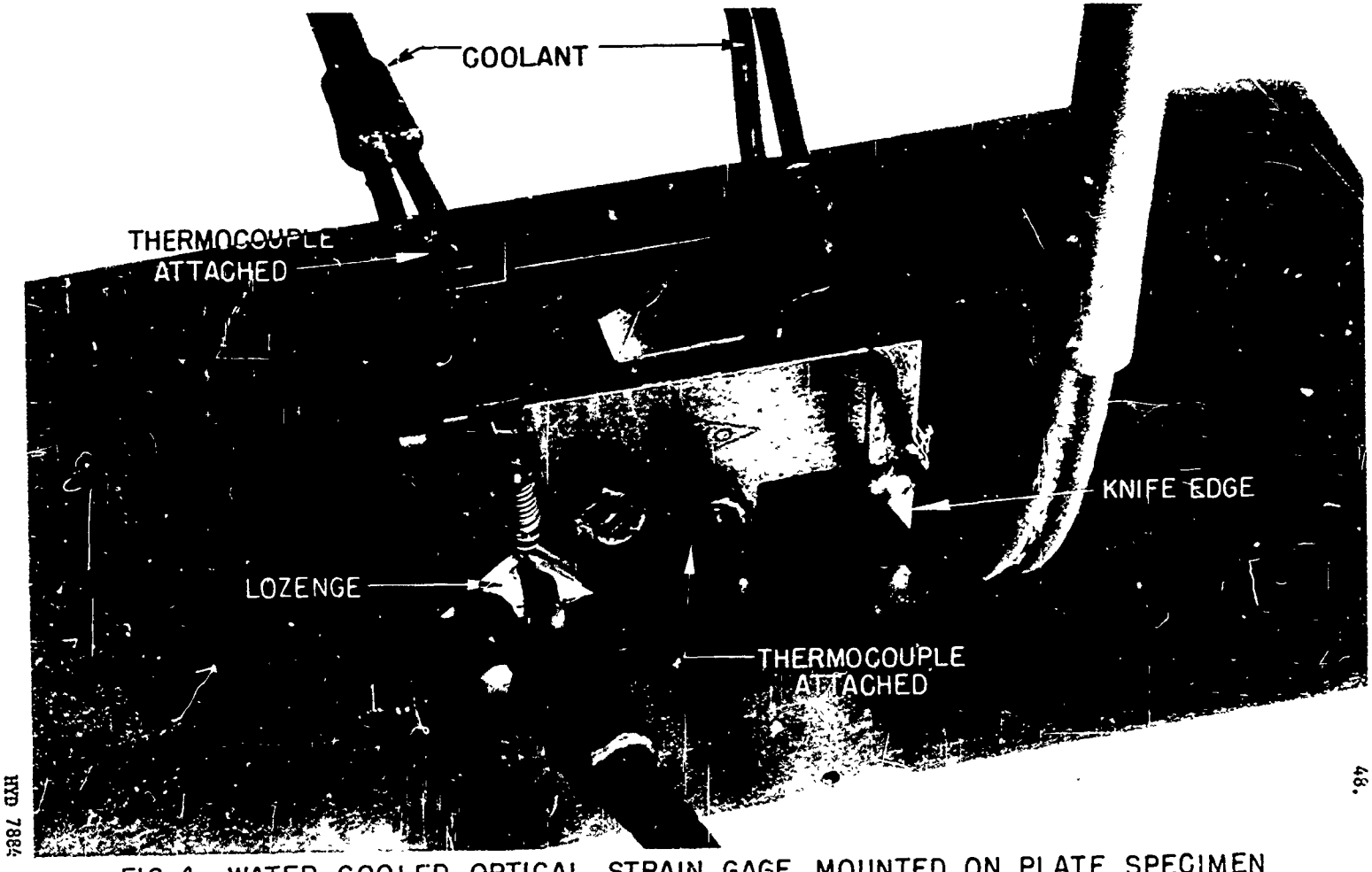

HWD 7884

FIG. 4 WATER COOLED OPTICAL STRAIN GAGE MOUNTED ON PLATE SPECIMEN

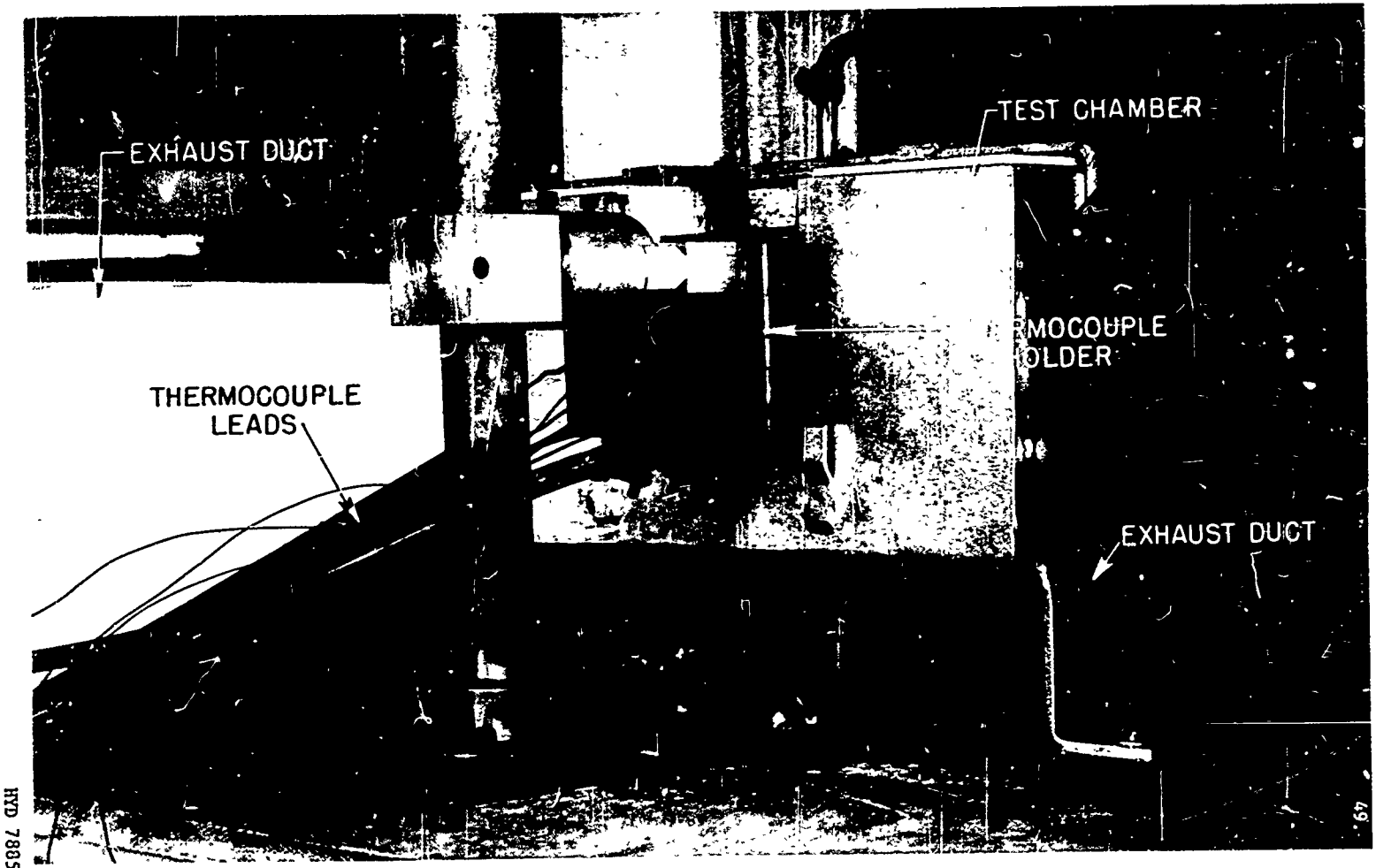

HXD 7885

FIG.5 TEST ARRANGEMENT FOR MEASUREMENT OF TEMPERATURE DISTRIBUTIONS

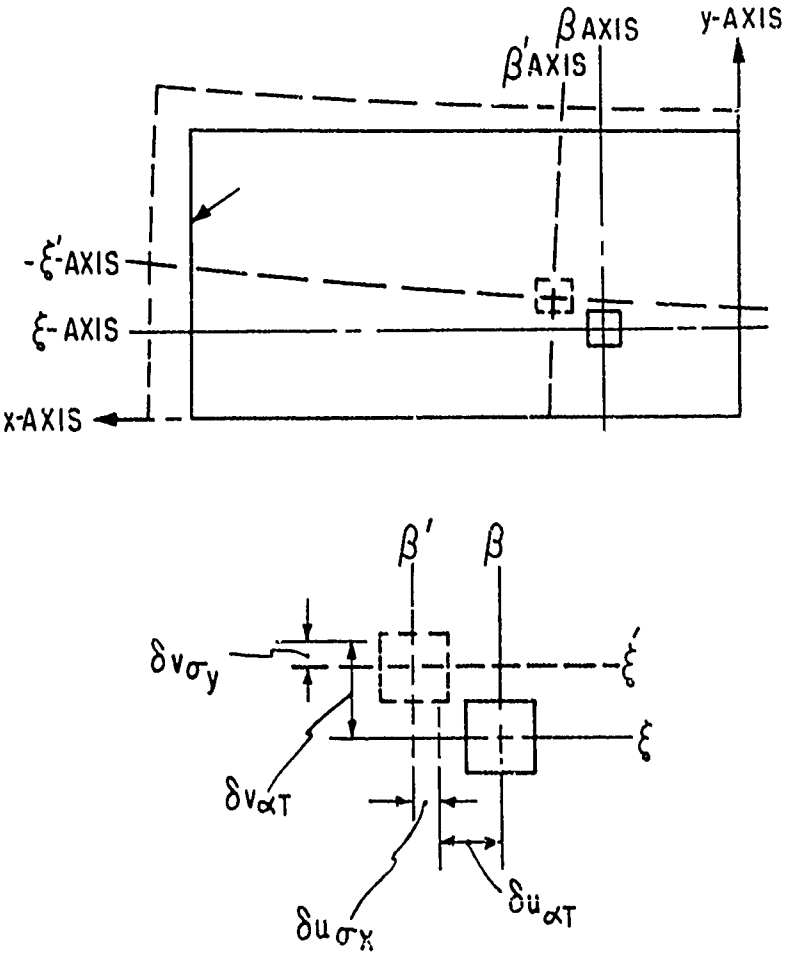

FIG 6 INITIAL AND FINAL PLATE QUADRANT SHAPE SHOWING AXES AND ELEMENT DISPLACEMENTS

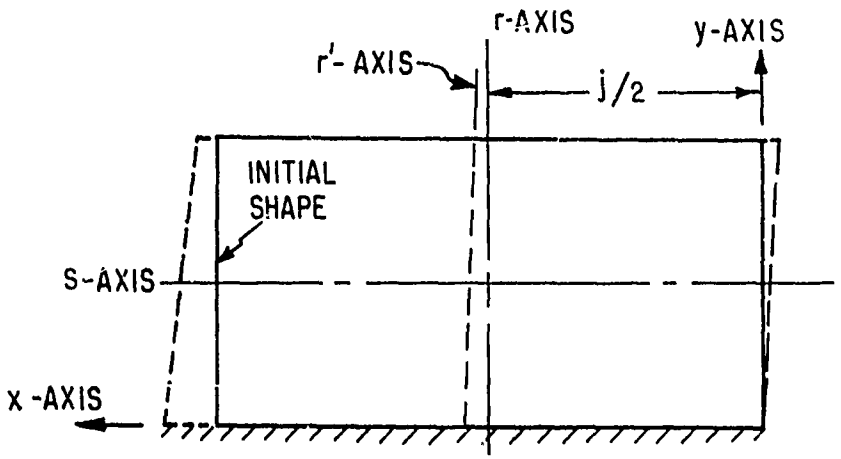

FIG. 7a INITIAL AND DISPLACED PLATE QUADRANT SHOWING BEAM ACTION IN Y-DIRECTION

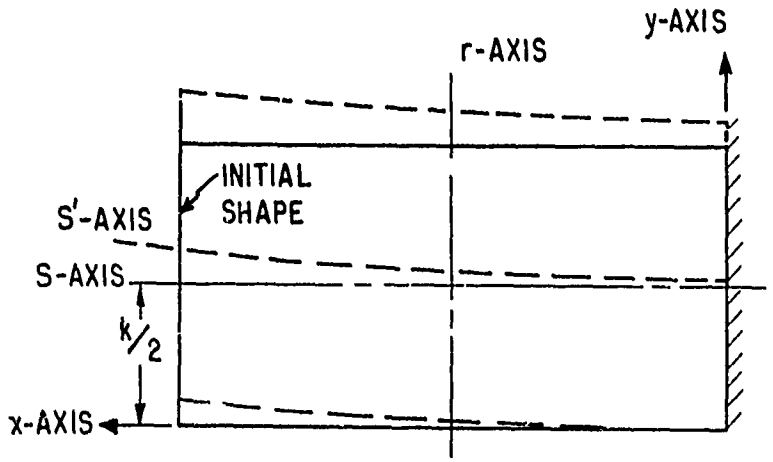

FIG. 7b INITIAL AND DISPLACED PLATE QUADRANT SHOWING BEAM ACTION IN X-DIRECTION

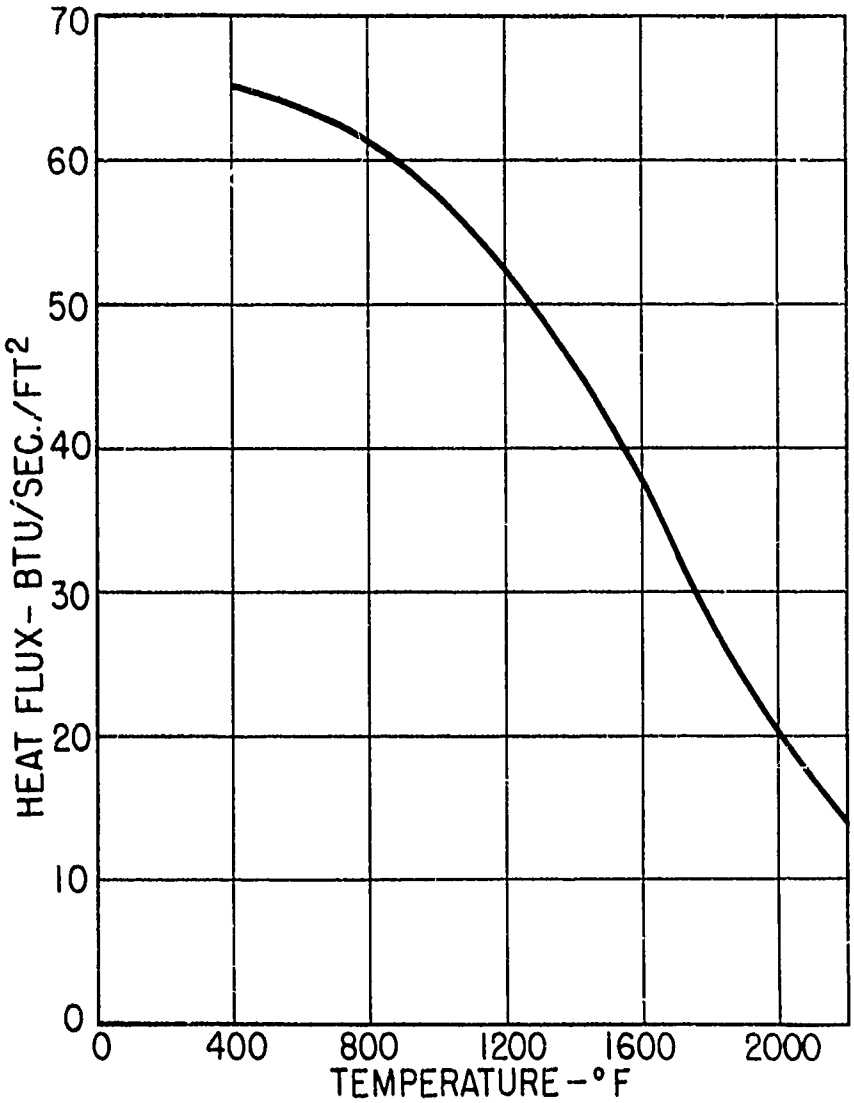

FIG. 8 HEAT FLUX INTO SPECIMEN AS A FUNCTION OF TEMPERATURE AT THE INTERSECTION OF THE x-AND y-AXIS OF TYPE 304 STAINLESS STEEL PLATE

HYD 7888

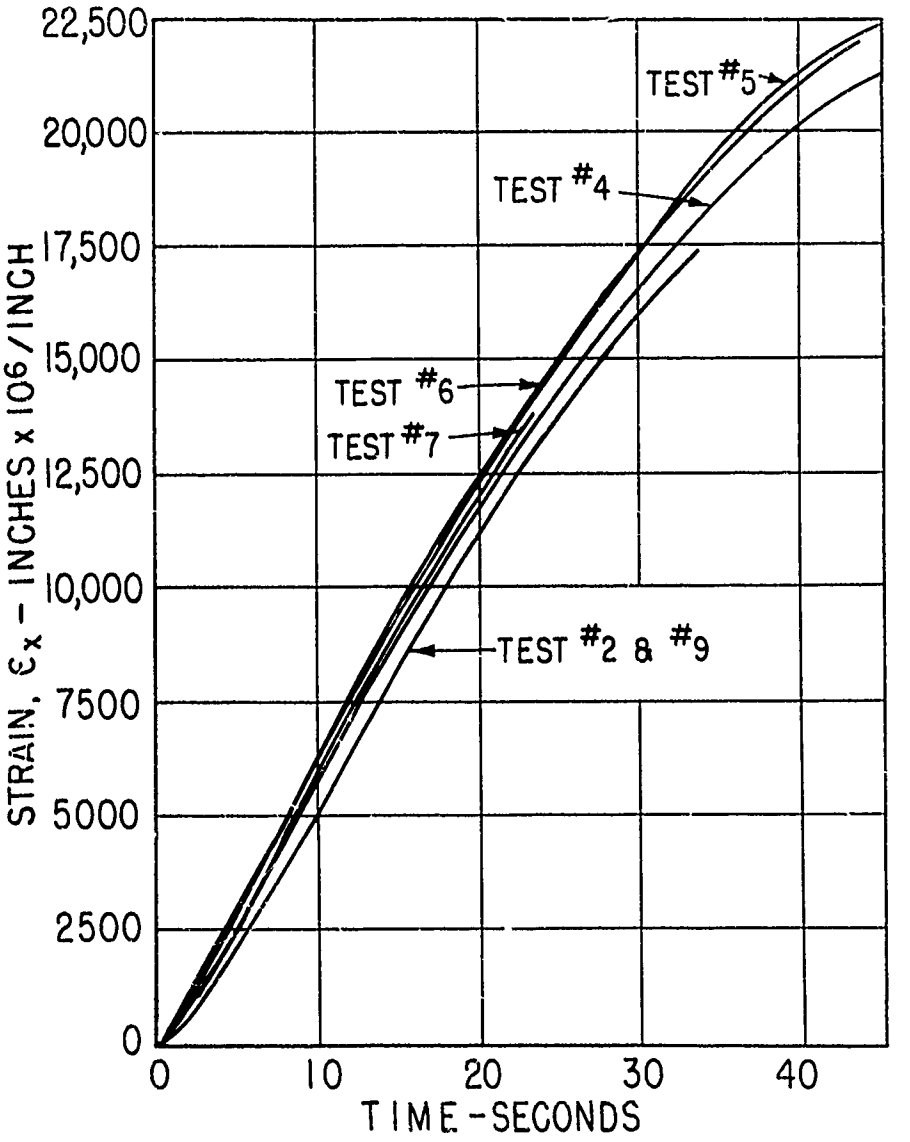

FIG.9 EXPERIMENTAL OPTICAL STRAIN MEASUREMENTS vs. TIME FOR HEATED TYPE 304 STAINLESS STEEL PLATES

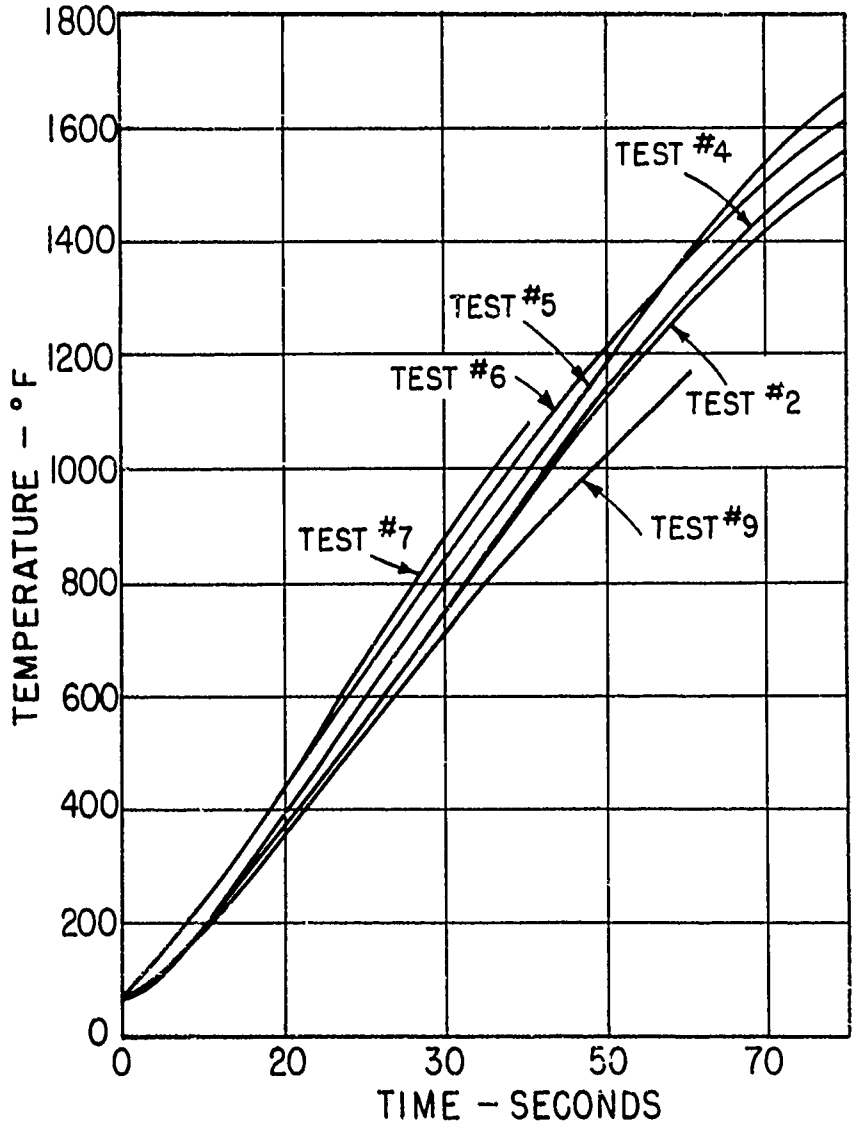

FIG. 10 EXPERIMENTAL TEMPERATURE MEASUREMENTS ON UNHEATED SURFACE OF TYPE 304 STAINLESS STEEL PLATES (x=-25/32", y = 11/16")

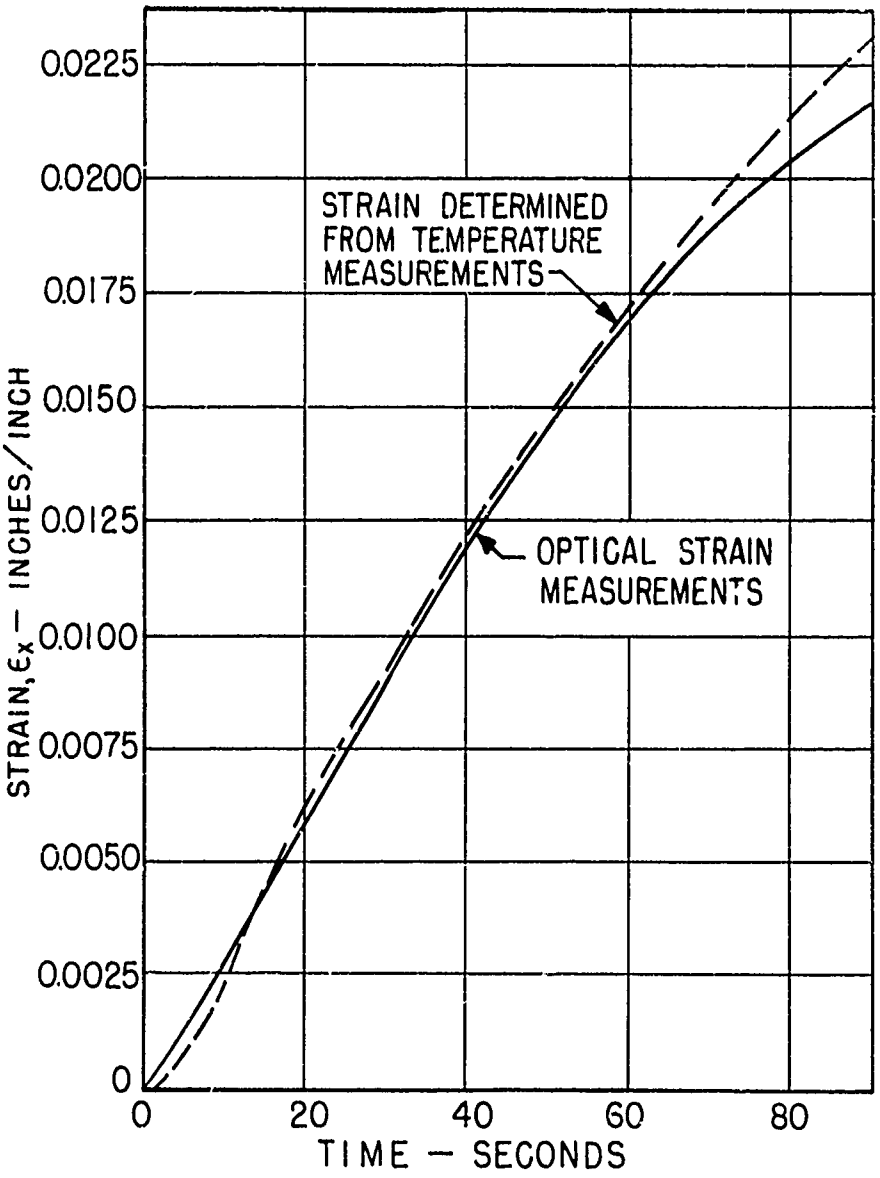

FIG.11 COMPARISON OF EXPERIMENTAL AND CALCULATED STRAINS vs TIME FOR TYPE 304 STAINLESS STEEL PLATE

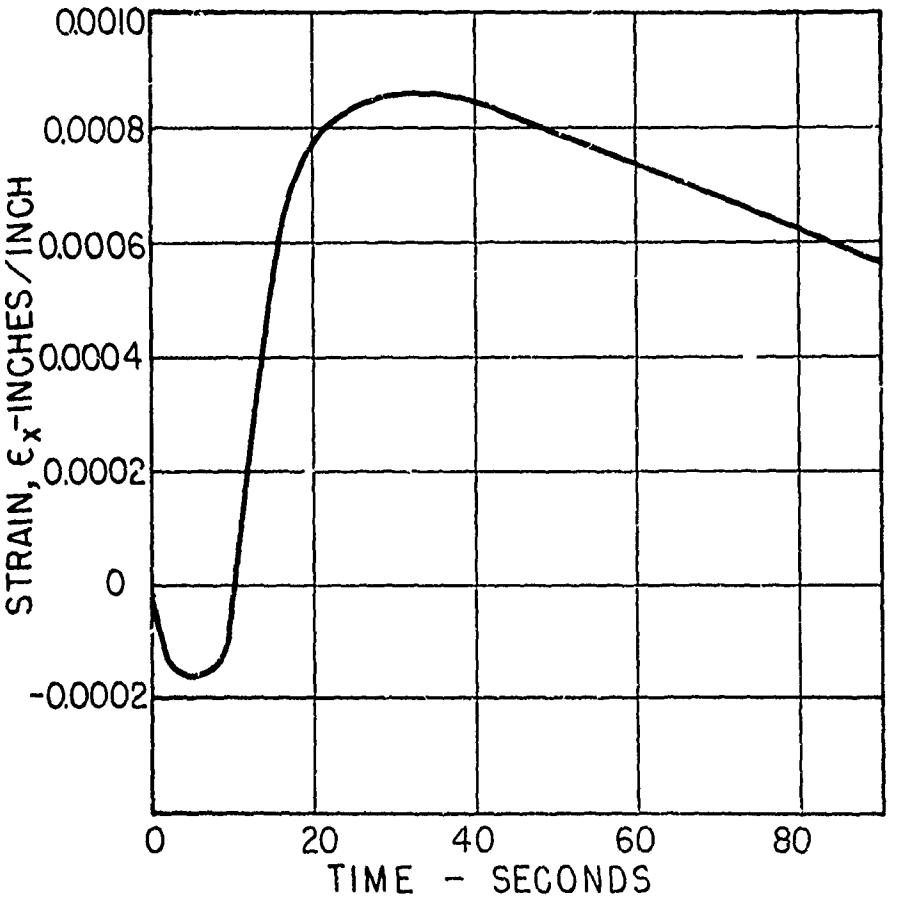

FIG. 12 NET STRAIN ON UNHEATED SURFACE BASED ON STRESS DISTRIBUTION vs TIME FOR TYPE 304 STAINLESS STEEL PLATE

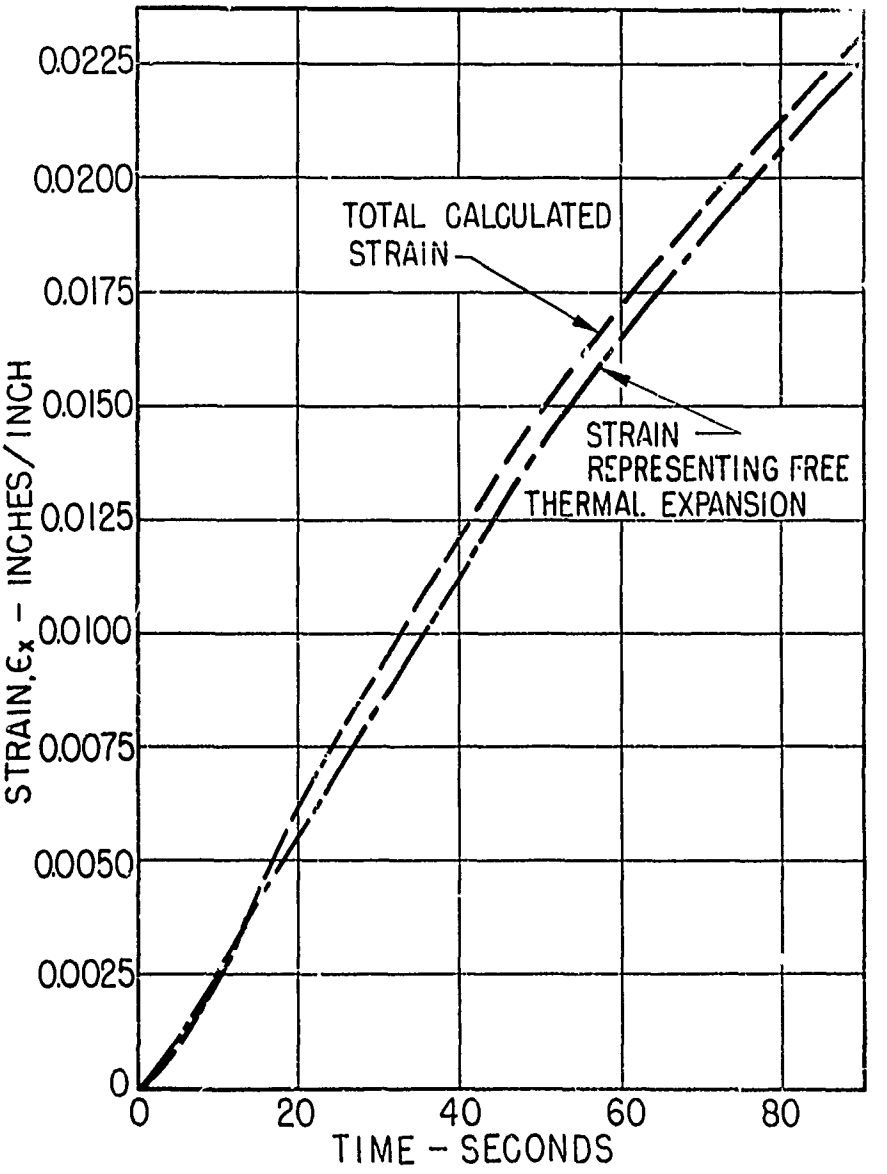

FIG.13 COMPARISON OF TOTAL CALCULATED STRAIN AND THE STRAIN DUE TO FREE THERMAL EXPANSION vs TIME FOR TYPE 304 STAINLESS STEEL PLATE

HYD 7893

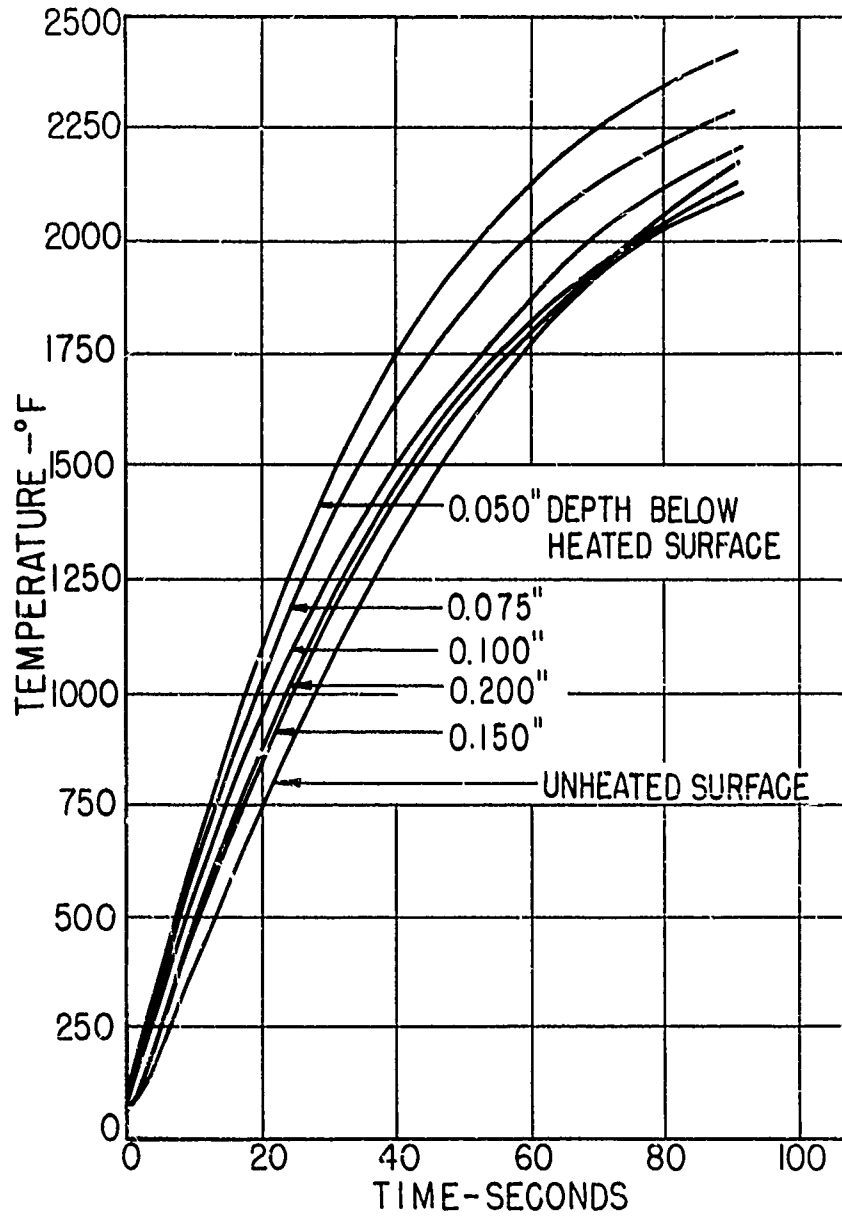

FIG. 14 TYPICAL TEMPERATURE RISE CURVES vs TIME AT VARIOUS DEPTHS BELOW HEATED SURFACE ($x = 1\frac{25}{32}$", y=0)

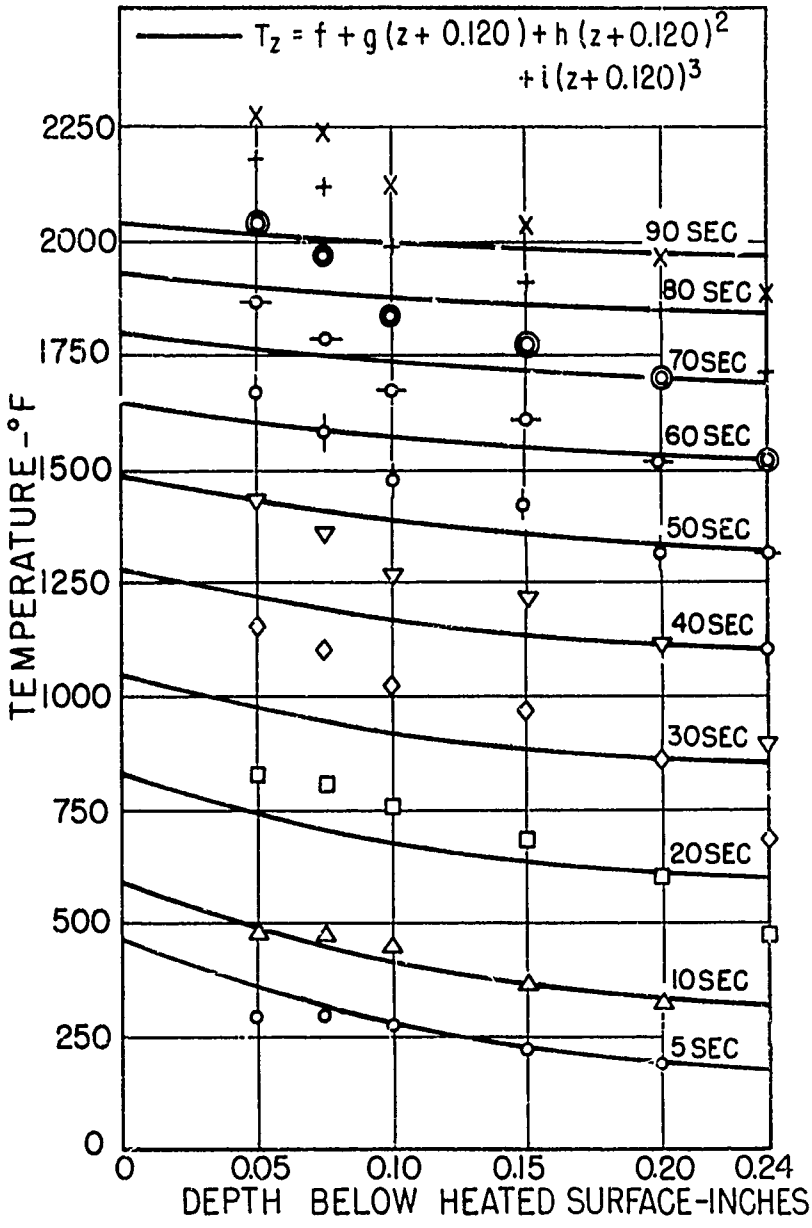

FIG. 15 TEMPERATURE DISTRIBUTION vs DEPTH BELOW HEATED SURFACE AT VARIOUS TIMES ($y = 0$, $x = 0$)

HYD 7895

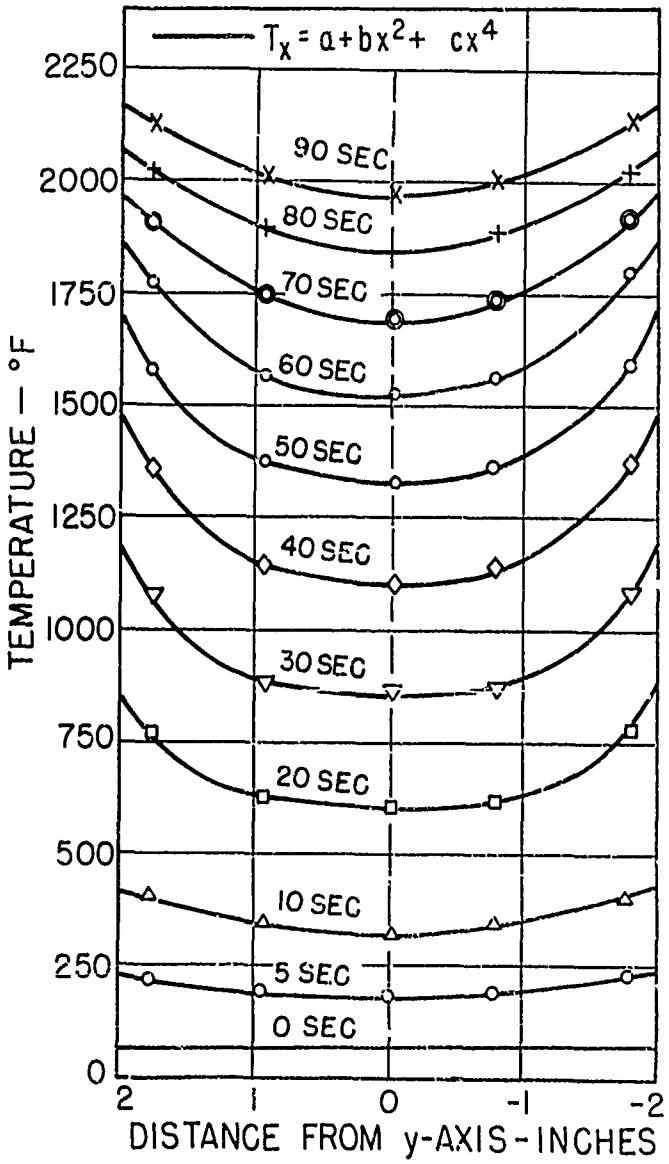

FIG. 16 TEMPERATURE DISTRIBUTION AT VARIOUS TIMES ALONG x-AXIS ON UNHEATED SURFACE (y = 0)

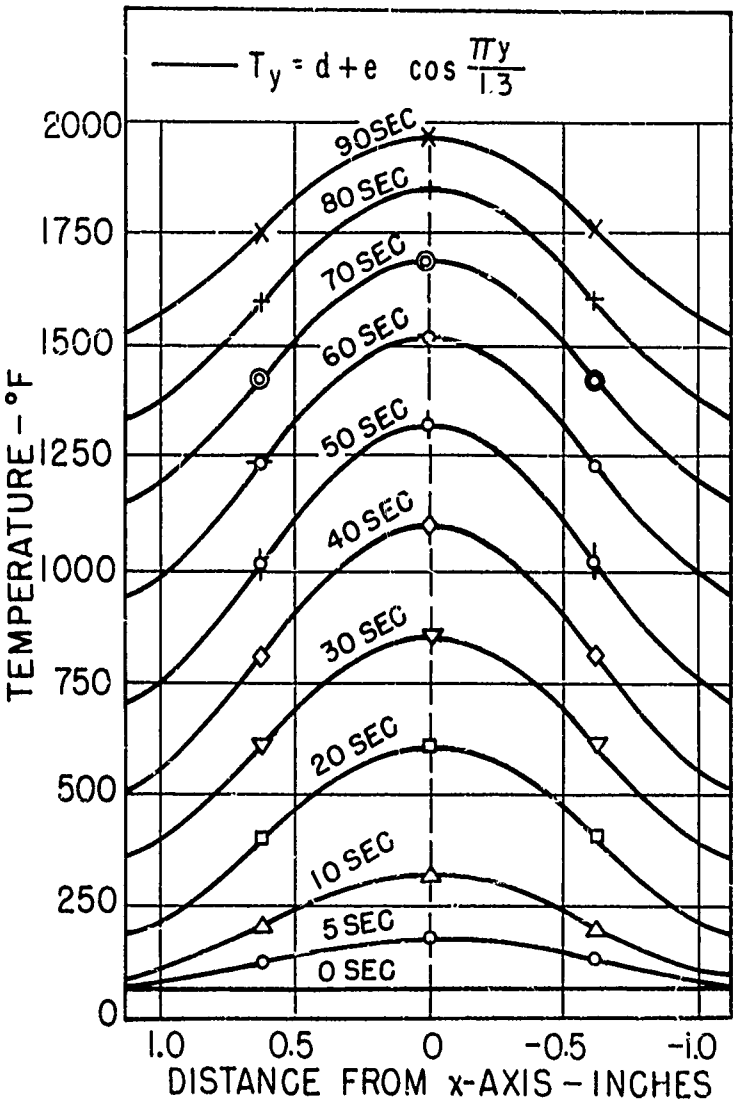

FIG. 17 TEMPERATURE DISTRIBUTION AT VARIOUS TIMES ALONG y-AXIS ON UNHEATED SURFACE (x = 0)

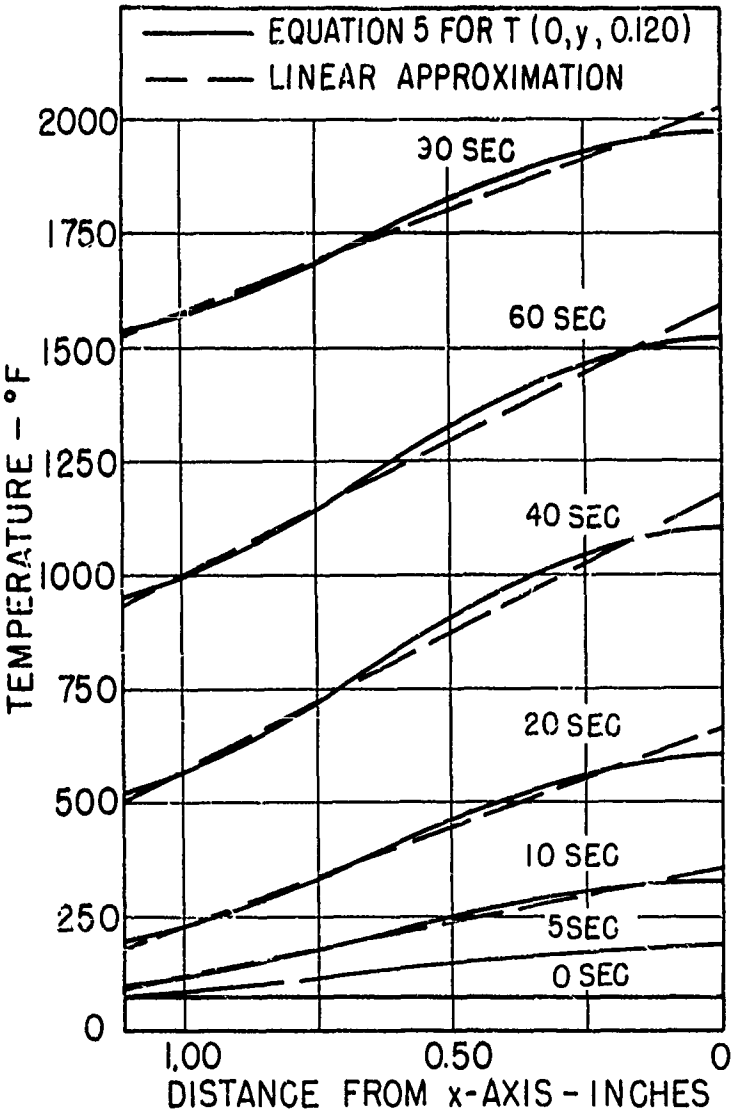

FIG. 18 TYPICAL TEMPERATURE DISTRIBUTION AT VARIOUS TIMES ALONG y-AXIS ON UNHEATED SURFACE (x = 0)

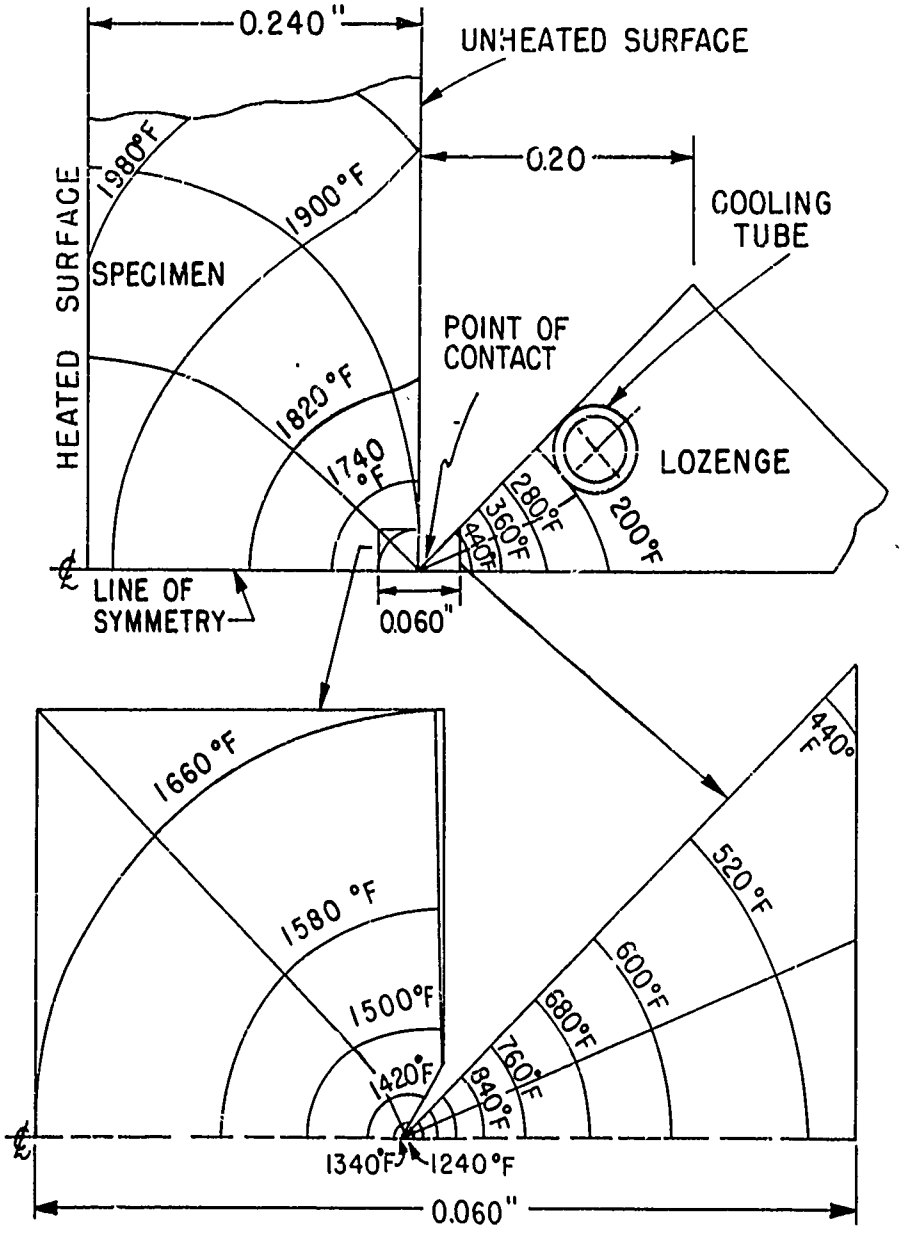

NOTE: THERMOCONDUCTIVITY OF LOZENGE AND SPECIMEN ARE ASSUMED EQUAL. A 100 °F TEMPERATURE DROP IS ASSUMED AT CONTACT POINT

FIG. 19 STEADY STATE TEMPERATURE DISTRIBUTION IN CONTACT AREA BETWEEN SPECIMEN AND STRAIN GAGE LOZENGE

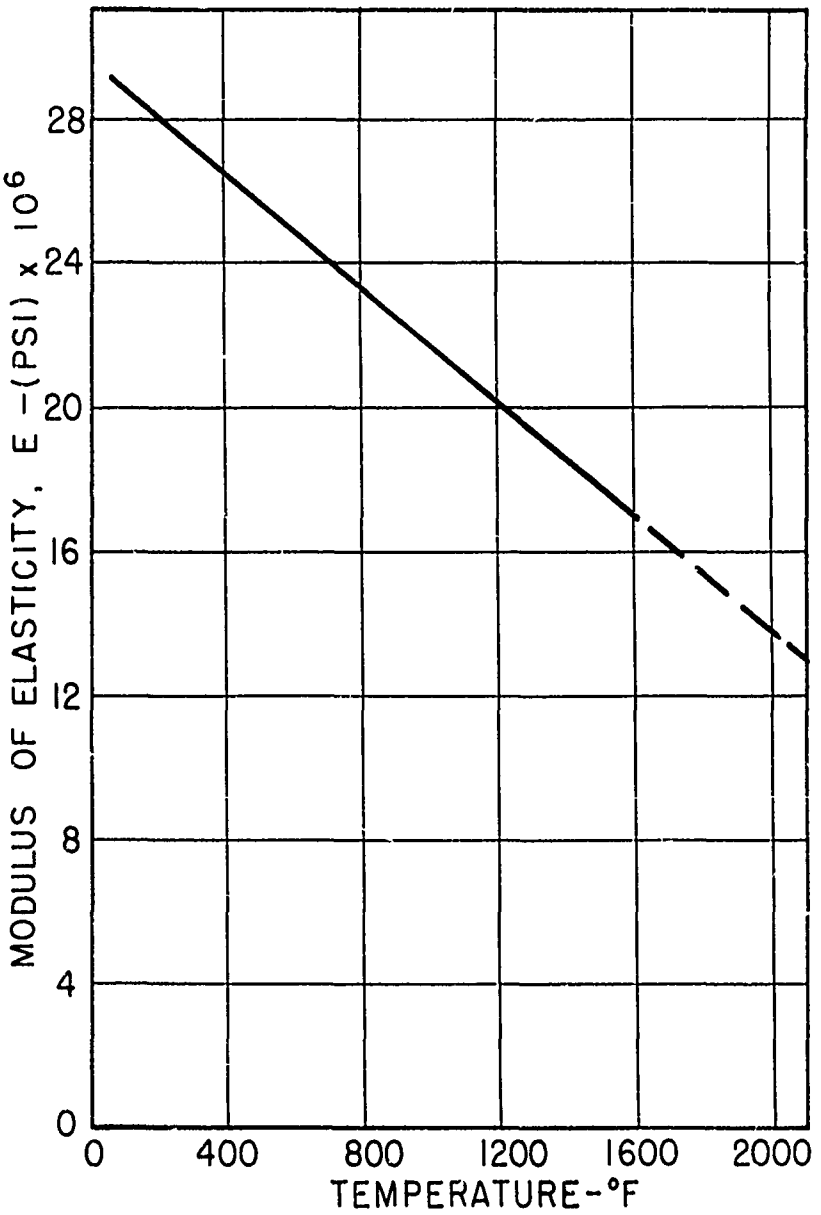

FIG. 20 MODULUS OF ELASTICITY vs TEMPERATURE IN TYPE 304 STAINLESS STEEL

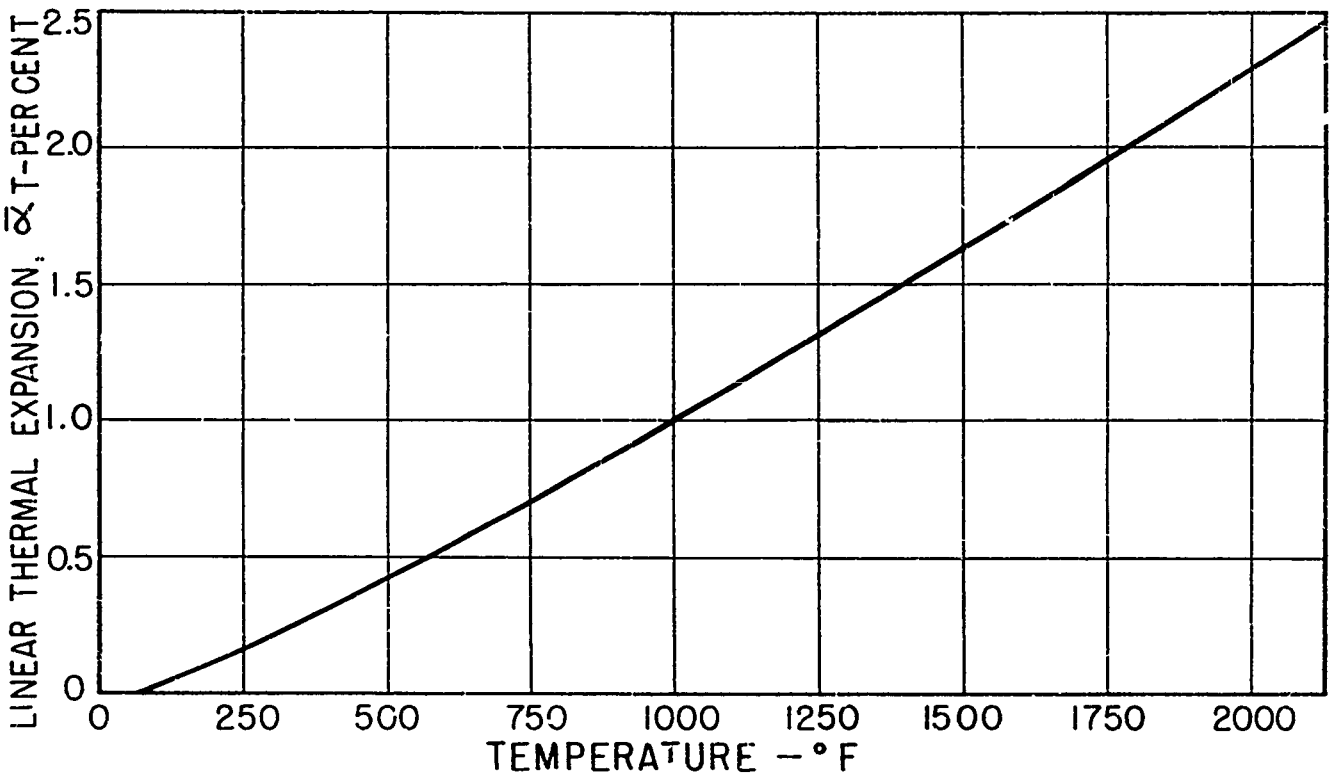

FIG. 21 LINEAR THERMAL EXPANSION FOR TYPE 304 STAINLESS STEEL

HED 7901

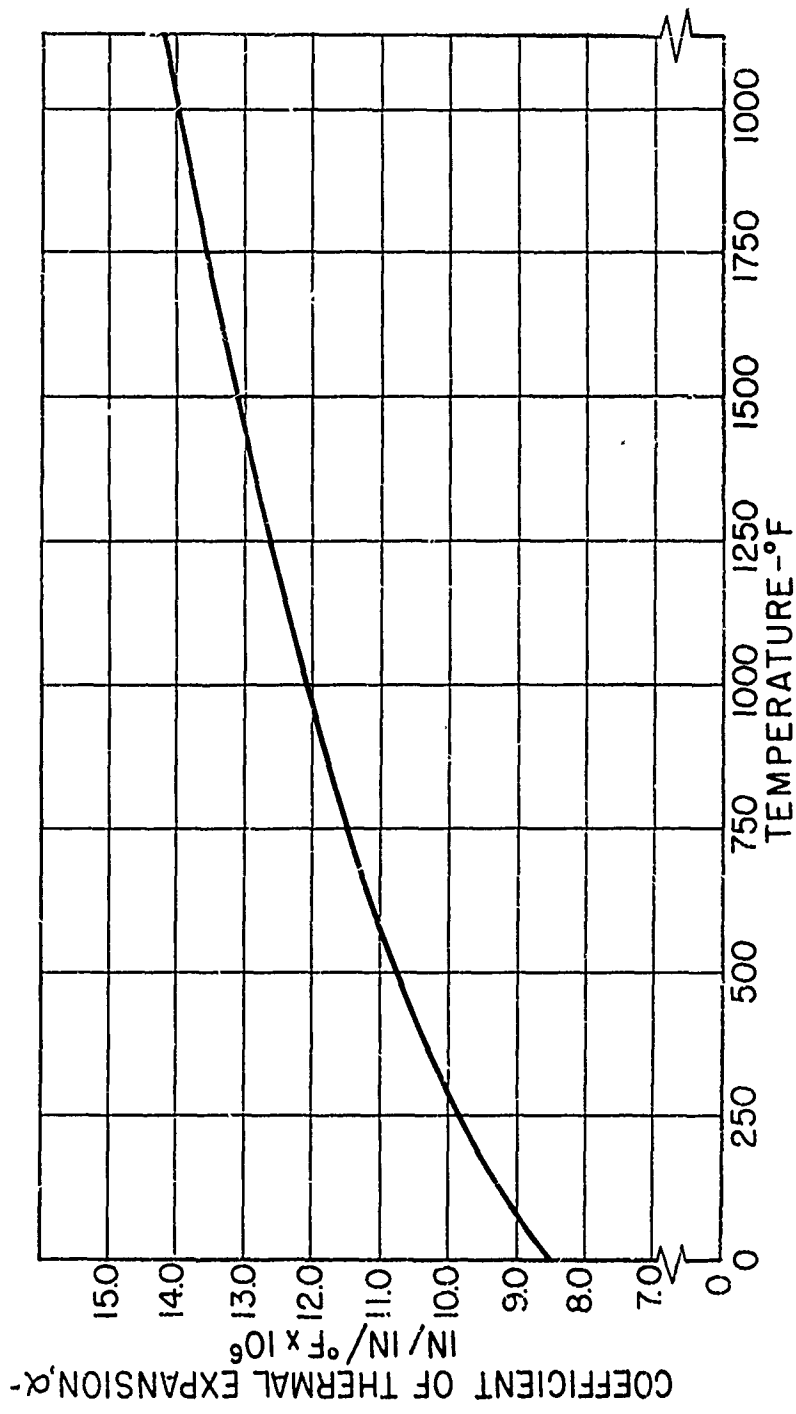

FIG. 22 COEFFICIENT OF THERMAL EXPANSION FOR TYPE 304 STAINLESS STEEL

HYD 7902

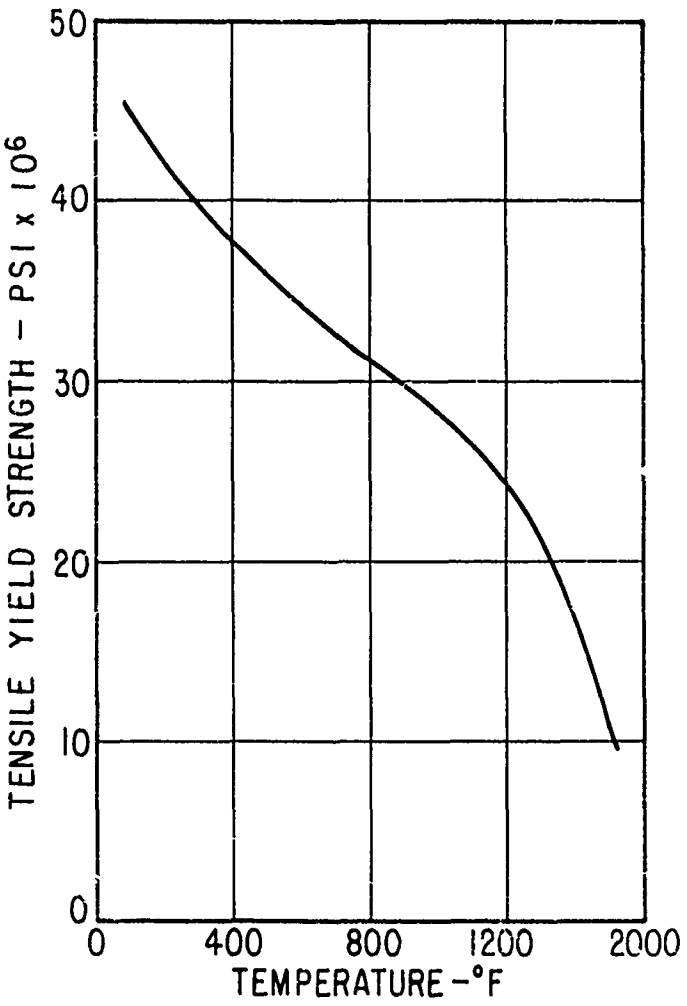

FIG.23 TENSILE YIELD STRENGTH OF TYPE 304 STAINLESS STEEL AS A FUNCTION OF TEMPERATURE

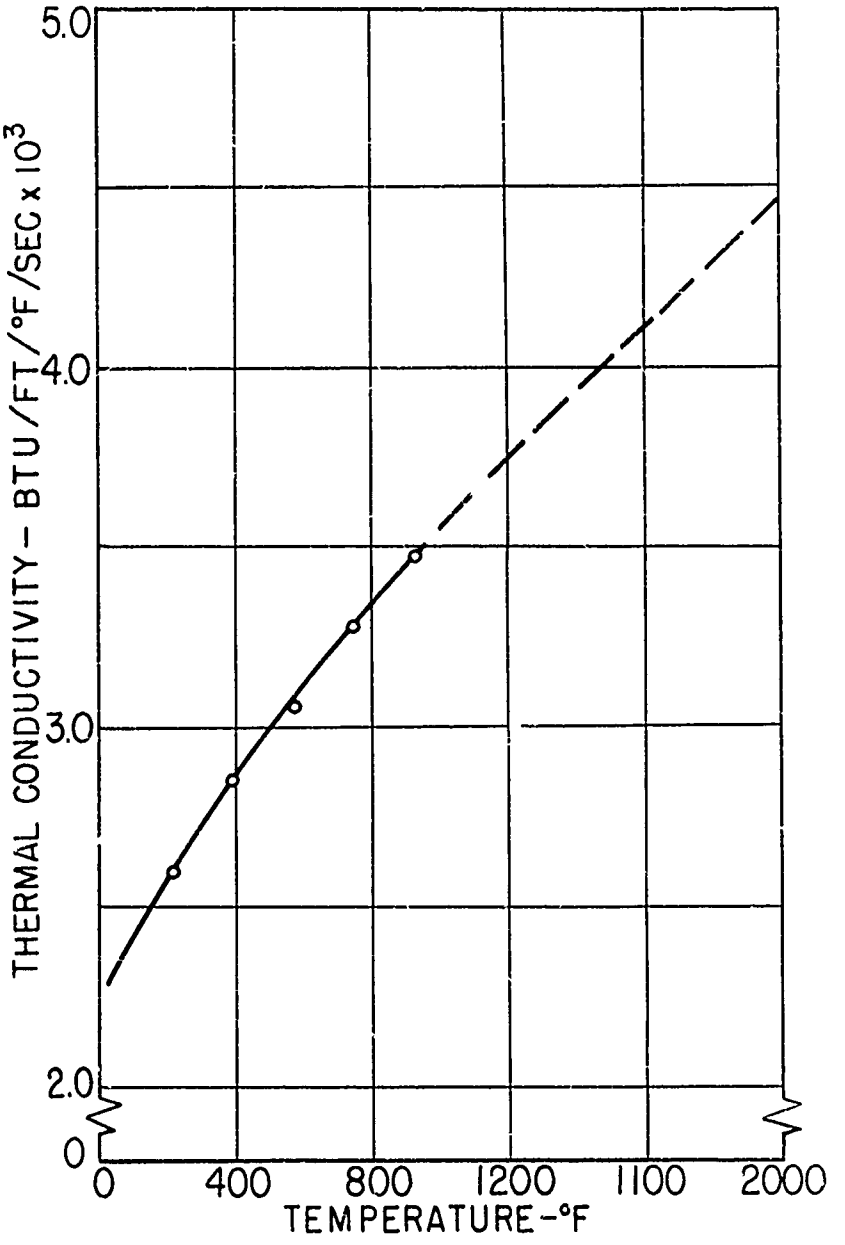

FIG.24 THERMAL CONDUCTIVITY vs TEMPERATURE FOR TYPE 304 STAINLESS STEEL

HYD 7904

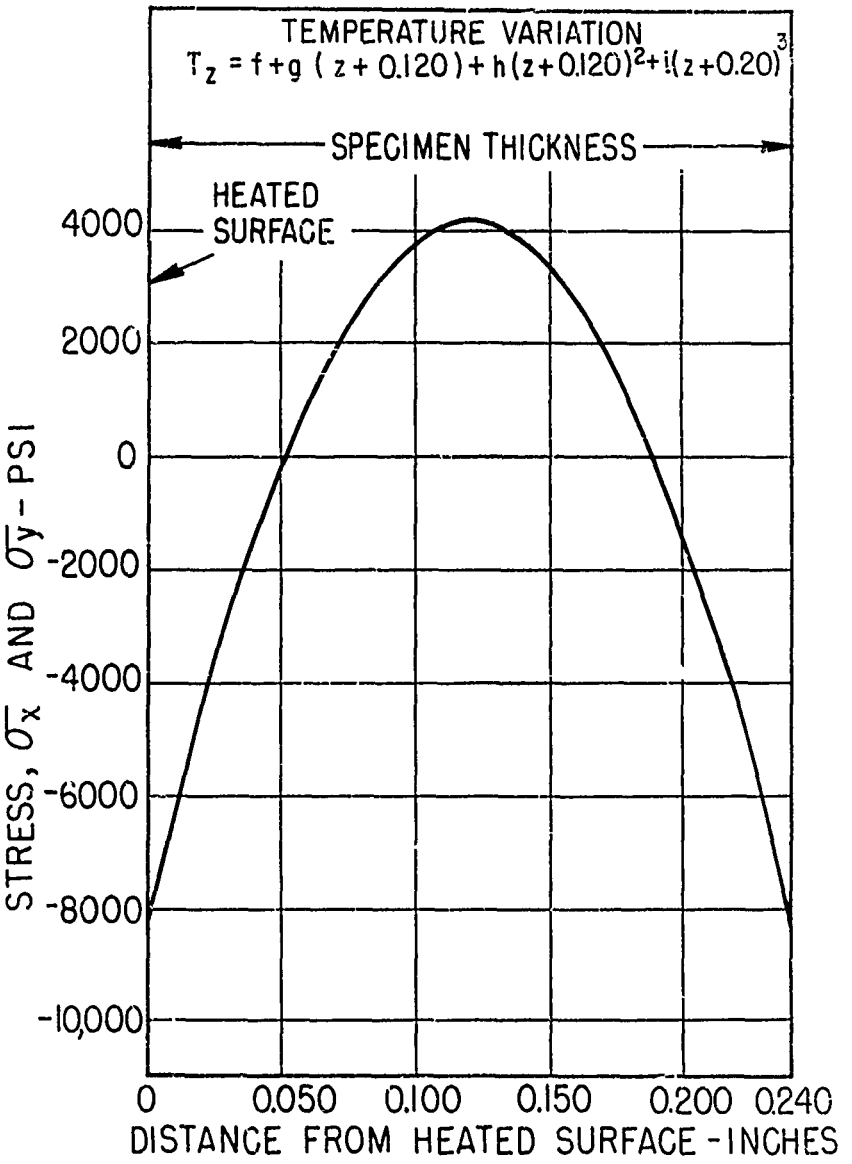

FIG.25 CACULATED STRESS DISTRIBUTION SPECIMEN THICKNESS BASED ON TEMPERATURE T_z AT x=0, y=0 AT 40 SECONDS

HYD 7905

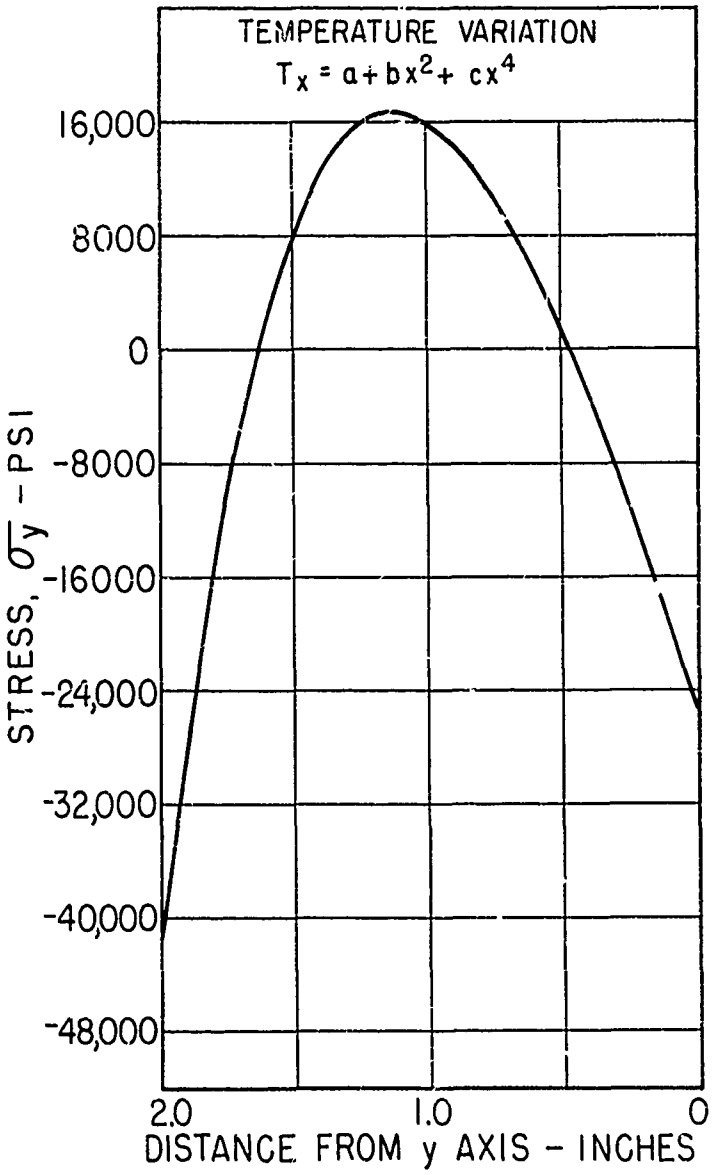

FIG. 26 CALCULATED STRESS DISTRIBUTION ON UNHEATED SURFACE OF SPECIMEN QUADRANT BASED ON TEMPERATURE T_x AT $y = 0$ AT 40 SECONDS

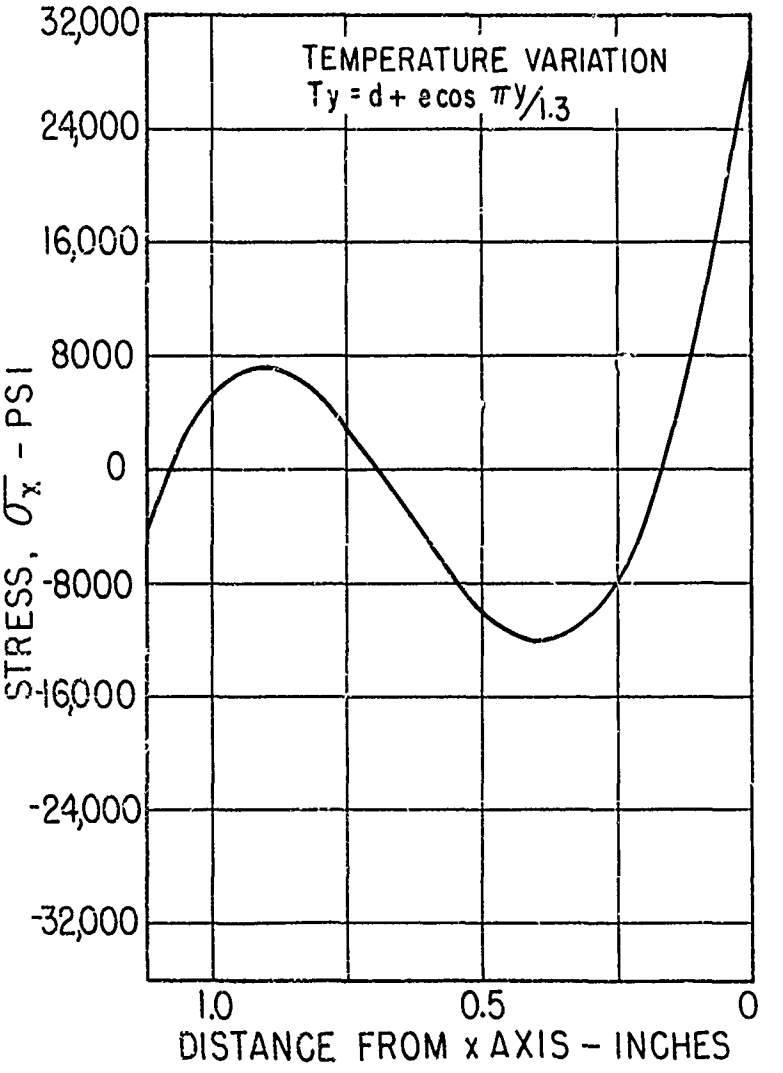

FIG. 27 CALCULATED STRESS DISTRIBUTION ON UNHEATED SURFACE OF SPECIMEN QUADRANT BASED ON TEMPERATURE Ty AT x = 0 AT 40 SECONDS

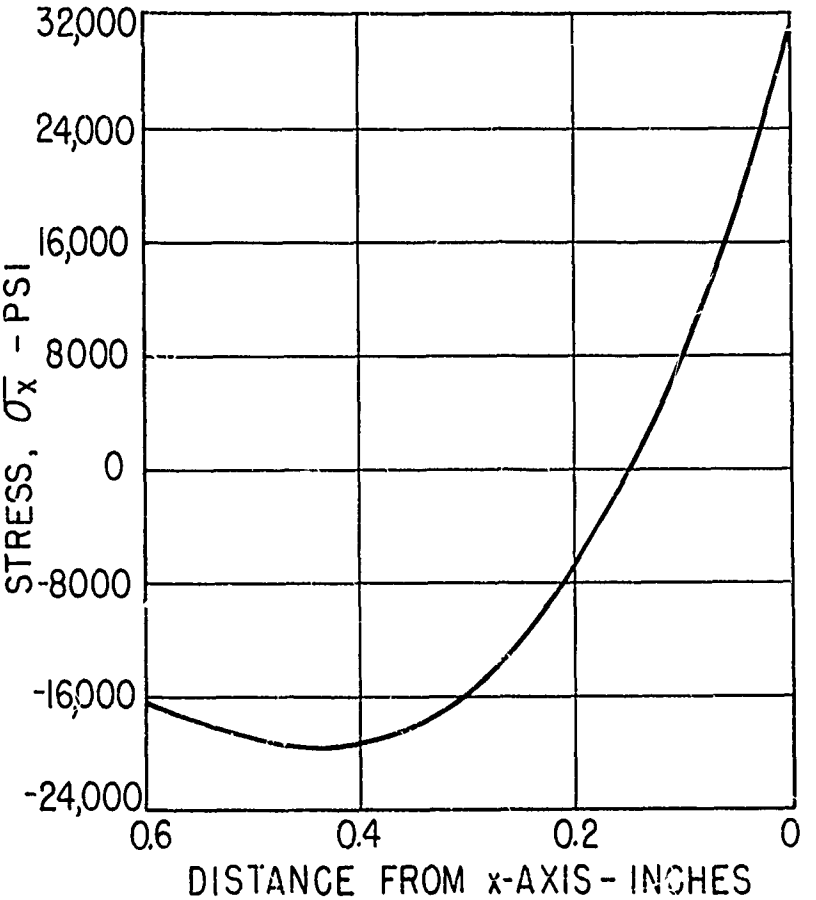

FIG. 28 STRESS DISTRIBUTION ON UNHEATED SURFACE OF SPECIMEN QUADRANT ALONG y-AXIS AT 40 SECONDS

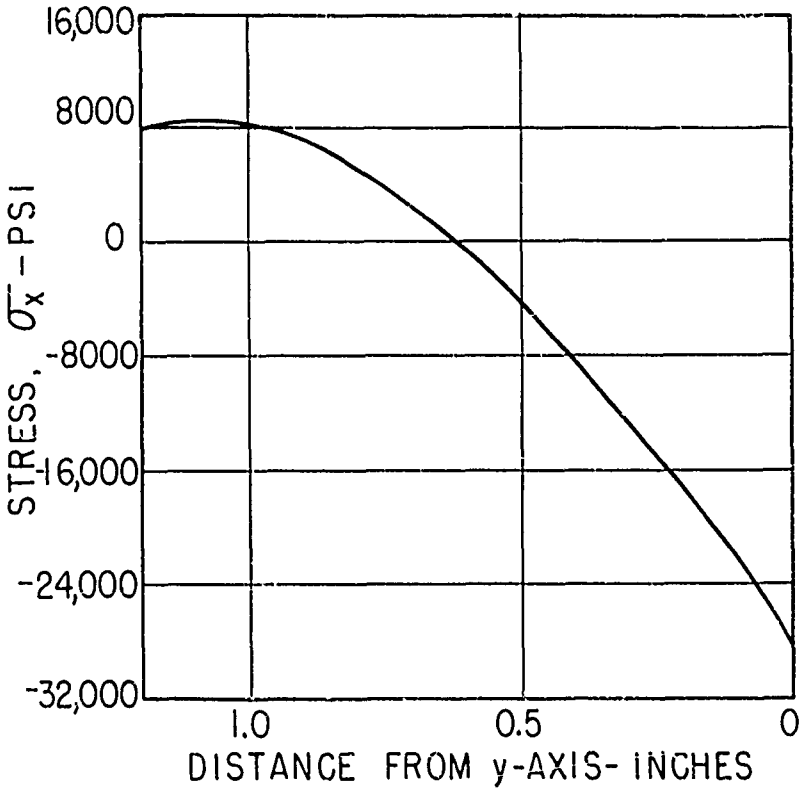

FIG. 29 STRESS DISTRIBUTION ON UNHEATED SURFACE OF SPECIMEN QUADRANT ALONG x-AXIS AT 40 SECONDS